Postnatal development of dendritic calcium signaling in rat hippocampal pyramidal cells

- Inauguraldissertation -
zur
Erlangung der Würde eines Doktors der Philosophie
vorgelegt der
Philosophisch-Naturwissenschaftlichen Fakultät
der Universität Basel

von

Jörg Pohle[1]
aus Dortmund, Deutschland

Basel, 2013

[1]E-Mail: joerg.pohle (with) gmx.de, joerg.pohle (with) gmail.com

Genehmigt von der Philosophisch-Naturwissenschaftlichen Fakultät auf Antrag von

Dissertationsleiter:	Prof. Dr. Josef Bischofberger Department of Biomedicine Pestalozzistrasse University of Basel Pestalozzistrasse 20 CH - 4056 Basel
Fakultätsverantwortlicher:	Prof. Dr. Peter Scheiffele Biozentrum University of Basel Klingelbergstrasse 50 / 70 CH - 4056 Basel
Korreferent:	Prof. Dr. Josef Kapfhammer Department of Biomedicine Pestalozzistrasse University of Basel Pestalozzistrasse 20 CH - 4056 Basel

Basel, den 23. April 2013

Prof. Dr. Jörg Schibler

Dekan der Philosophisch-
Naturwissenschaftlichen Fakultät

creative commons

Namensnennung-Keine kommerzielle Nutzung-Keine Bearbeitung 2.5 Schweiz

---

Sie dürfen:

das Werk vervielfältigen, verbreiten und öffentlich zugänglich machen

Zu den folgenden Bedingungen:

Namensnennung. Sie müssen den Namen des Autors/Rechteinhabers in der von ihm festgelegten Weise nennen (wodurch aber nicht der Eindruck entstehen darf, Sie oder die Nutzung des Werkes durch Sie würden entlohnt).

Keine kommerzielle Nutzung. Dieses Werk darf nicht für kommerzielle Zwecke verwendet werden.

Keine Bearbeitung. Dieses Werk darf nicht bearbeitet oder in anderer Weise verändert werden.

- Im Falle einer Verbreitung müssen Sie anderen die Lizenzbedingungen, unter welche dieses Werk fällt, mitteilen. Am Einfachsten ist es, einen Link auf diese Seite einzubinden.
- Jede der vorgenannten Bedingungen kann aufgehoben werden, sofern Sie die Einwilligung des Rechteinhabers dazu erhalten.
- Diese Lizenz lässt die Urheberpersönlichkeitsrechte unberührt.

Quelle: http://creativecommons.org/licenses/by-nc-nd/2.5/ch/ Datum: 3.4.2009

Contents

1 Abstract **6**

2 Introduction **7**

2.1 Hippocampus 7

2.1.1 Significance of hippocampus 7

2.1.2 CA1 pyramidal neurons 10

2.1.3 Postnatal development of place cells 11

2.1.4 Dendritic development from an anatomical viewpoint 13

2.2 Immaturity of pyramidal cells in one week old rats 14

2.3 Ca^{2+} in dendritic development 14

2.4 Dendritic backpropagation of action potentials 16

2.5 Age-dependency of Ca^{2+} extrusion mechanisms 18

2.6 The aims of this work 19

3 Materials and Methods **20**

3.1 Slice preparation 20

3.2 Electrophysiology 20

3.3 Fluorescent measurements 21

3.3.1 Stray-light factor method 22

3.4 Calibration of ratiometric Ca^{2+} measurements 23

3.5 Data analysis 23

3.6 Linear compartment model 24

3.6.1 Influx 24

3.6.2 Ca^{2+} buffering 25

3.6.3 Ca^{2+} clearance from the cytosol 27

3.6.4 Calcium dynamics 27

3.6.5 Solution of equation for one-compartment model 27

3.6.6 Consequences of the one-compartment-model 28

3.7 Modelling of linear dendritic Ca^{2+} signaling during short bursts . . 30

3.8 Modelling of non-linear Ca^{2+} signaling during theta bursts firing . . 30

3.9 Statistics 31

3.10 Age binning 31

4 Results **32**

4.1 Active dendritic backpropagation in young CA1 pyramidal cells . . 32
4.2 Postnatal development of Ca^{2+} buffering and extrusion 37
4.3 Linear summation of Ca^{2+} transients during brief bursts of APs . . 40
4.4 Activity dependent slow-down of Ca^{2+} extrusion during theta-burst firing 43
4.5 Supra-linear summation of dendritic Ca^{2+} signals in young CA1 pyramidal cells 46

5 Discussion **49**
5.1 Ca^{2+} handling of young neurons 49
5.2 Non-linear Ca^{2+} summation 51
5.3 Ca^{2+} buffer capacity in interneurons and principal neurons 53
5.4 Possible mechanisms of slow-down of Ca^{2+} extrusion 56
5.5 Functional role of activity-dependent slow-down 57

Bibliography **60**

List of Figures **67**

List of Tables **69**

Nomenclature **70**

1 Abstract

In CA1 pyramidal neurons, dendritic Ca^{2+} transients in stratum radiatum were evoked in acute slices via backpropagating action potentials using patch clamp recordings.

Although Ca^{2+} is critically important for activity-dependent neuronal development, not much is known about the regulation of the dendritic Ca^{2+} signals in developing neurons. Here we used ratiometric Ca^{2+} imaging to investigate dendritic Ca^{2+} signalling in rat hippocampal pyramidal cells during the first 1 to 4 weeks of postnatal development, focussing on a comparison of 1 week vs 4 weeks old rats. We show for the first time that active dendritic backpropagation of Na_v-channel dependent action potentials (APs) evoked already large dendritic Ca^{2+} transients in one-week-old animals with amplitudes of ∼140 nM similar to mature pyramidal cells (∼160 nM). Although, AP-evoked dendritic calcium load increases ∼4 times during the first 4 weeks (∼10 µM versus ∼40 µM), this seems to be out-balanced by a ∼3.5-times increase in Ca^{2+} buffer capacity κ_S (∼70 versus ∼240). Furthermore, linear summation of Ca^{2+} transients in young and mature cells during brief bursts of APs was similar. Surprisingly, repetitive theta-burst stimulation for two seconds showed ∼2.5-times larger dendritic Ca^{2+} signals in 1 week-old rats than predicted by linear summation and was about ∼2-3-times larger than measured in 4 weeks old rats. We could show that this non-linear summation of Ca^{2+} transients was due to an activity-dependent slow-down of Ca^{2+} extrusion in the young neurons. Taken together, the data suggest that active backpropagation regulate dendritic Ca^{2+} signals already during early postnatal development. Remarkably, Ca^{2+} signals in young neurons are even several times larger than in mature cells due to activity dependent regulation of Ca^{2+} extrusion rates. Extrusion rates are slower in young neurons compared to mature neurons, 4.5-times for single APs and up to 8-times at the end of theta-burst stimulation.

2 Introduction

2.1 Hippocampus

2.1.1 Significance of hippocampus

The hippocampus belongs to the medial temporal lobe memory system (Fig. 2.1AB) and gets sensory inputs via perirhinal cortex, parahippocampal cortex and entorhinal cortex (Fig. 2.1C). The hippocampus consists of several regions, namely the dentate gyrus, CA3, CA1, and the subiculum (Fig. 2.2A). The hippocampus plays a crucial role in explicit memory formation and spatial navigation. The famous patient H.M. was removed much of his temporal lobes bilaterally. After this surgery he was cured from his epilepsy but missing the ability to form new explicit memories, an anterograde amnesia. However, his working memory stayed intact. H.M. long-term memory deficits were constricted to the retrieval of facts and events regardless of the sensory modality, but not motor skills (implicit memories) (Purves et al. 2008).

The major route of information flow follows the so-called trisynaptic pathway from dentate gyrus to CA3 to CA1 to subiculum and back to entorhinal cortex (Fig. 2.2B). In addition to the trisynaptic, there are several 'short cut' pathways, with direct projections from the entorhinal cortex to CA3 and to CA1 pyramidal cells (direct pathway). Of course this view is lacking the large number of GABAergic interneurons synchronizing the activity of the principal cells (Bartos et al. 2002).

At the cellular level learning and memory is thought to be a modification of synaptic plasticity (Feldman 2012), dendritic plasticity (Briz et al. 2013), spine plasticity (Lai, Franke, and Gan 2012; Vogel-Ciernia et al. 2013) or changed excitability of parts of the dendritic tree (Losonczy, Makara, and Magee 2008).

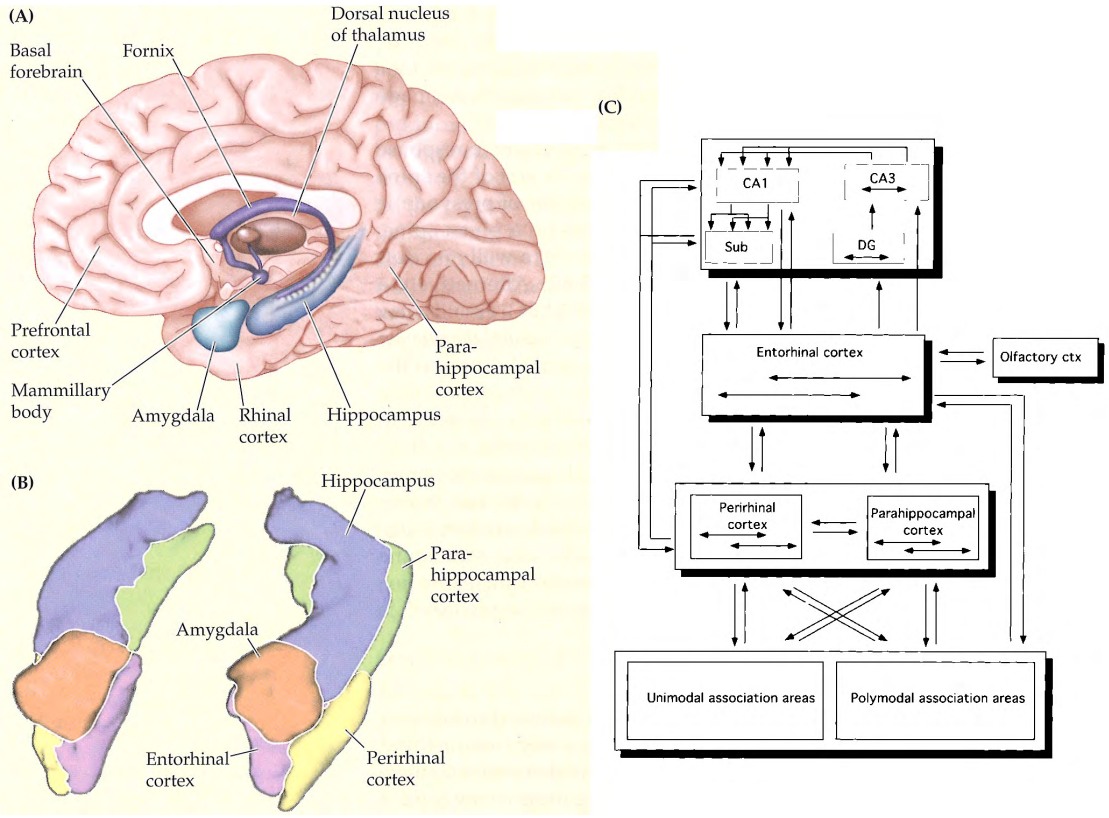

Figure 2.1: **A** Location of medial temporal lobe regions within the human brain. **B** 3D view of the subregions of the medial temporal lobe. **C** Neural connections among medial temporal lobe regions and between these regions and the rest of the brain. Figures and legends from Purves et al. 2008; Lavenex and Amaral 2000.

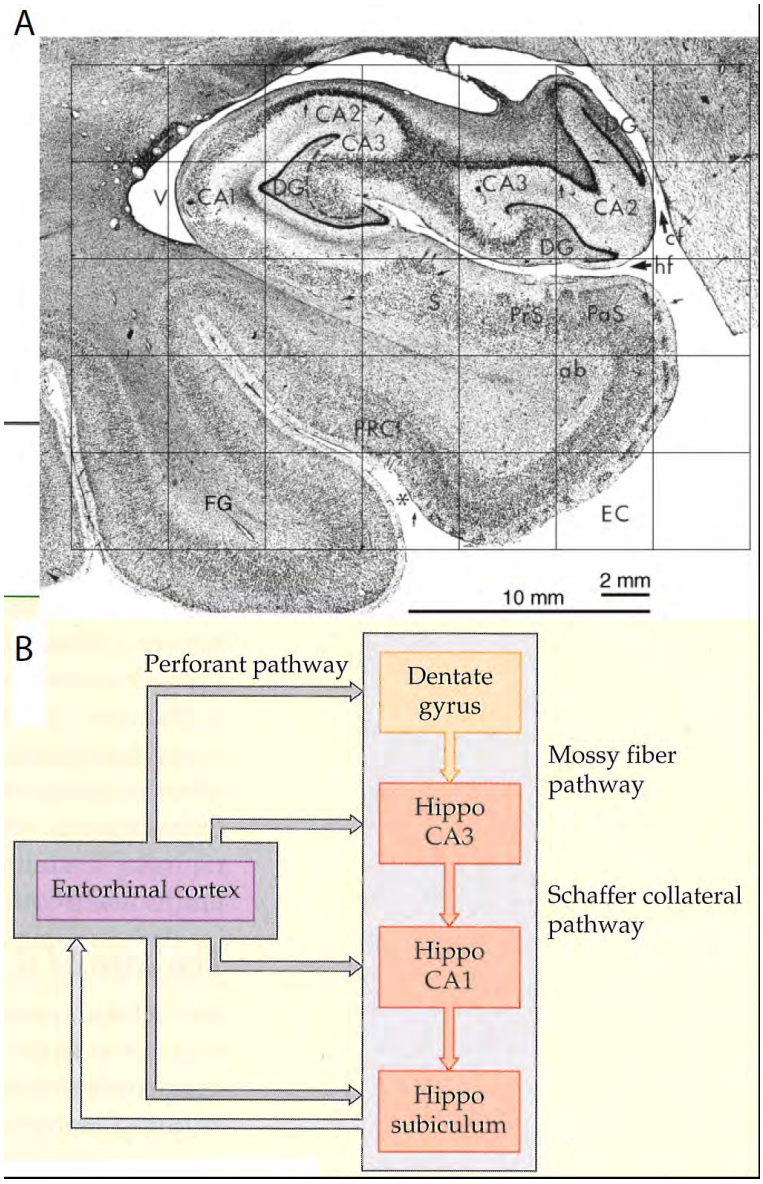

Figure 2.2: **A** Morphology of hippocampus. Nissl-stained coronal section. DG=dentate gyrus, EC=entorhinal cortex, FG=fusiform gyrus, hf=hippocampal fissure, PRC=perirhinal cortex, PaS=parasubiculum, PrS=presubiculum, S=subiculum. **B** Connections within the subregions of the hippocampus, including the entorhinal-dentate-CA-subiculum-entorhinal loop. Figures and legends from Purves et al. 2008; Amaral 1999.

2.1.2 CA1 pyramidal neurons

Most of the pyramidal neurons in the CA1 region of the mature hippocampus are place cells (Langston et al. 2010; Wills et al. 2010). During spatial exploration they fire action potentials (APs) only if animals cross a specific region in the environment, the so-called place field of the specified neuron. Furthermore, firing is temporally modulated by theta rhythm (∼5-10 Hz). As a consequence, pyramidal cells fire single spikes at the border and brief bursts of APs in the middle of their place field.

The place cells fire with a certain phase shift related to the theta rhythm. When the rat enters the place field, firing starts at the peak of theta oscillation. When the rat crosses the place field, the cells's bursting rate is a little higher than the overall theta rhythm, thus the cell's firing moves towards earlier phases of the theta rhythm, until the cells's firing stops almost at the trough of theta rhythm, when the rats leaves the place field (Huxter, Burgess, and O'Keefe 2003). This phenomenon is called phase precession (Fig. 2.3) and potentially delivers an alternative, enhanced code for location and the duration within the place field.

If the spatial surroundings are changed at once, the hippocampal place cells representation flickers a few cycles between the old and the new representation (Jezek et al. 2011).

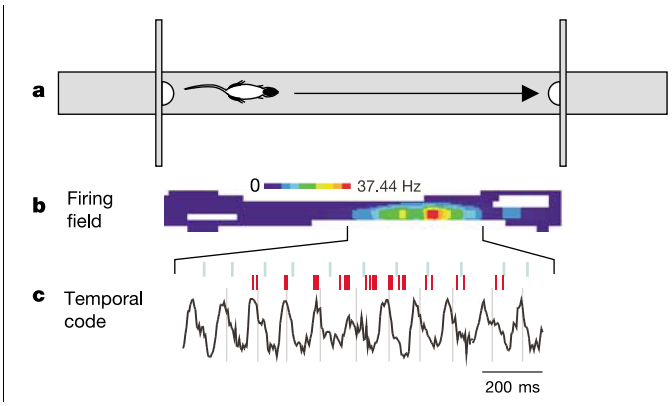

Figure 2.3: **a**: Attracted by food, a rats moves back and forth along a linear track. **b**: Place field of one place cell created from multiple runs into only one direction. **c**: EEG theta rhythm (in black) and place cell firing (in red) for the same cell on a single run. The cell's bursting rate is higher than EEG theta frequency causing each successive burst to move to an earlier phase of the theta cycle, despite initially rising, then falling firing rate. Figure and legend modified from Huxter, Burgess, and O'Keefe 2003.

CA1 pyramidal neurons receive their synaptic inputs in the stratum radiatum (Fig. 2.4), which owes its name to the many parallel apical dendrites of the CA1

neurons, by the Schaffer collaterals (axons) of the CA3 pyramidal cells (trisynaptic pathway). The dendritic tree of the CA1 pyramidal neurons further extends

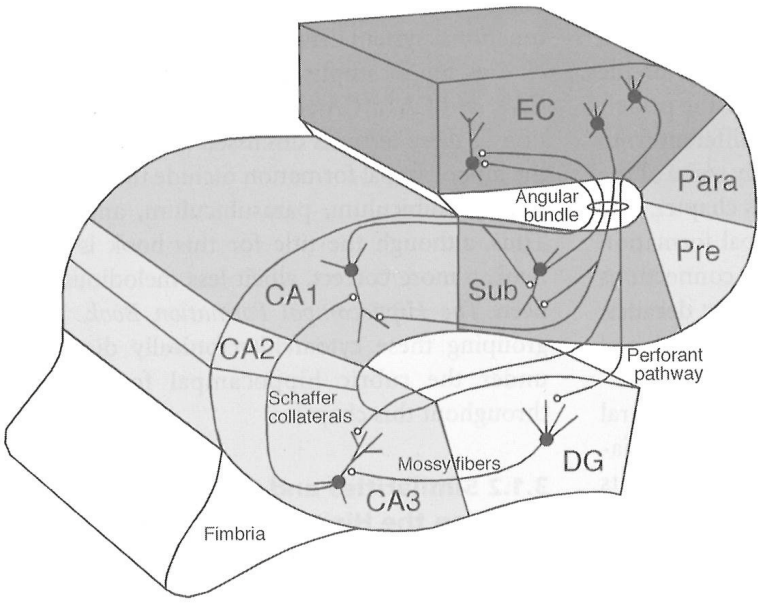

Figure 2.4: The hippocampal formation. Neurons in layer II of the entorhinal cortex project to the dentate gyrus and the CA3 field of the hippocampus proper via the perforant pathway. Neurons in layer III of the entorhinal cortex project to the CA1 field of the hippocampus and the subiculum via the perforant and alvear pathways. The granule cells of the dentate gyrus project to the CA3 field of the hippocampus via mossy fiber projections. Pyramidal neurons in the CA3 field of the hippocampus project to CA1 via Schaffer collaterals. Pyramidal cells in CA1 project to the subiculum. Both CA1 and the subiculum project back to the deep layers of the entorhinal cortex. Figure and legend from Andersen et al. 2006.

to stratum lacunosum moleculare. There, the CA1 pyramidal neurons receive different inputs mostly from entorhinal cortex (direct pathway).

The axons of the CA1 pyramidal neurons project to subiculum or back to entorhinal cortex.

2.1.3 Postnatal development of place cells

Langston et al. 2010 found that at P14-P16 41% of the CA1 pyramidal cells are place cells. This number increases to around 75% at P28-P30 and drops to 60% at P31-P35 reaching the adult fraction. Firing fields of CA1 place cells stabilize with age.

At P16-P18 the existing place cells are already theta-modulated and show phase-precession. To our knowledge, place field firing in one week old rats or other

animals has not been studied. However, the connections of the CA1 area of hippocampus to prefrontal cortex have been studied (Brockmann et al. 2011). Even at P7-P8 old rats, there are theta-phase locked CA1 pyramidal neurons interacting with prelimbic neurons in the prefrontal cortex (Fig. 2.5).

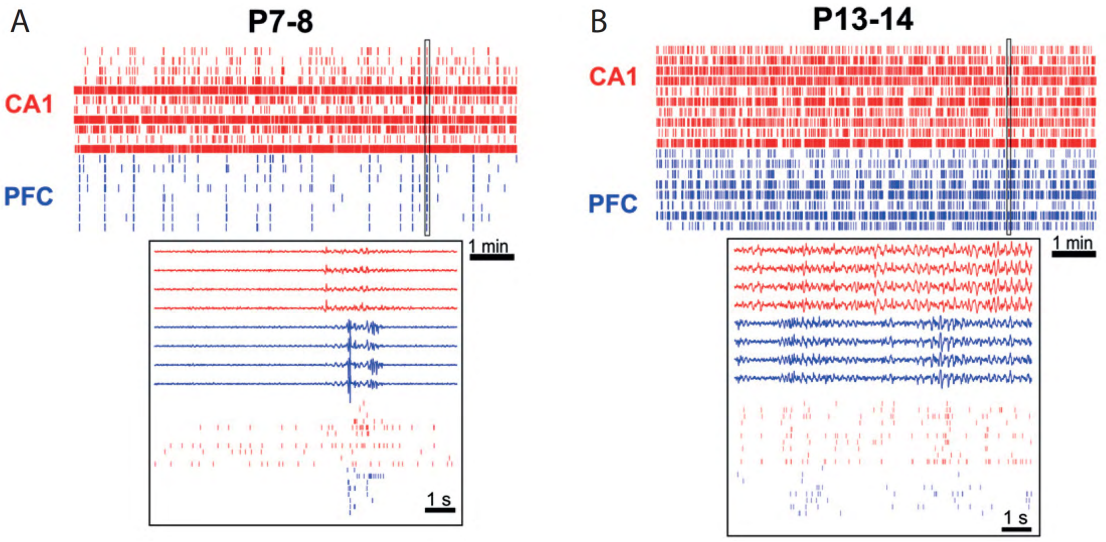

Figure 2.5: **A**: Spike trains from 11 CA1 (red) and 8 PL (blue) simultaneously recorded neurons from a P7 rat. Note the low firing rate of the immature prelimbic neurons. Inset, close-up of the spike trains shown in (A) displayed at enlarged time scale together with the corresponding field potential on four prelimbic and four hippocampal recording sites of the multitelectrode. **B**: Same as (A) for 10 CA1 (red) and 8 PL neurons (blue) from a P13 rat. Figure and legend from Brockmann et al. 2011.

2.1.4 Dendritic development from an anatomical viewpoint

Even at P7, the dendritic tree of (layer V) pyramidal cells already has the characteristic zones observed in older ages (Romand et al. 2011). The somata of reconstructed pyramidal neurons of different age are aligned at the bottom of Fig. 2.6, their basal dendrites are not shown. At P7, apical dendrites exhibit numerous short filopodia-like branchlets which disappear until P14. The apical dendritic tree rapidly grows and reaches about 90% of the adult length already at P14.

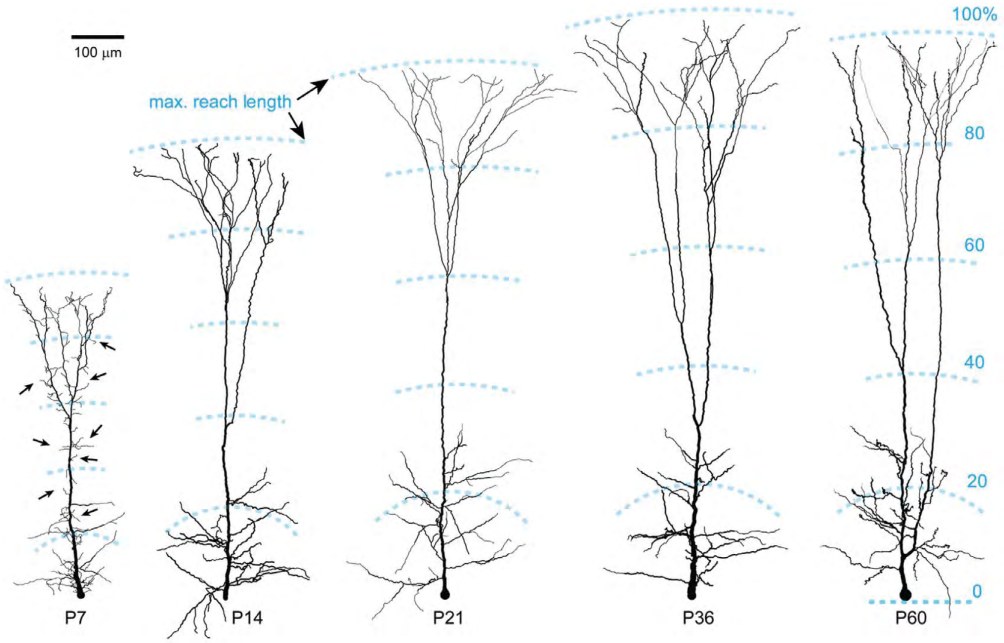

Figure 2.6: Developmental changes in the morphology of apical dendrite. Representative reconstructions of apical dendrites from different ages. Note the rapid growth of apical dendrites and the disappearance of filopodia-like branches (arrows) along the apical dendrite from P7 to P14. The structural frame kept similar over all ages with obliques distributed in the approximate 30% and tufts in the distal 20-30% of the maximal reach length. Figure and legend from Romand et al. 2011

2.2 Immaturity of pyramidal cells in one week old rats

Pyramidal neurons in one week old rats are surrounded by immature brain tissue. Astrocytes are known to be responsible for potassium buffering at synapses which are surrounded by astrocytic processes (Wallraff et al. 2006). But these astrocytes are still immature in one week old rats and express low levels of inward rectifier potassium channels Kir4.1 (Seifert et al. 2009) which are thought to be important for potassium homeostasis at the CA1 synapses.

Furthermore, one week old pyramidal cells exhibit less KCC2 (Sipilä et al. 2009), a chloride potassium symporter, which is important for cellular protection against excitotoxicity.

2.3 Ca^{2+} in dendritic development

At the age of one week, rats have to acquire somatosensory input with the help of their whiskers, their eyes only open around P12. How does the dendritic tree cope with the necessary activity to induce dendritic plasticity? Neuronal activity is of major importance during postnatal development for built-up of neuronal circuits (Katz and Shatz 1996; Hensch 2005b; Hensch 2005a; Ge et al. 2007).

Intracellular Ca^{2+} increase is important for dendritic development (Wong and Ghosh 2002; Konur and Ghosh 2005; Lohmann, Finski, and Bonhoeffer 2005; Spitzer 2006). Local Ca^{2+} signals regulate via Rho family proteins (Jin et al. 2005) dendritic branch dynamics and stability, whereas global Ca^{2+} signals regulate dendritic growth via transcriptional factors (Konur and Ghosh 2005; Fig. 2.7). Furthermore, elevations of intracellular Ca^{2+} concentration effects gene expression, neurotoxicity and dendritic excitability (Ghosh and Greenberg 1995).

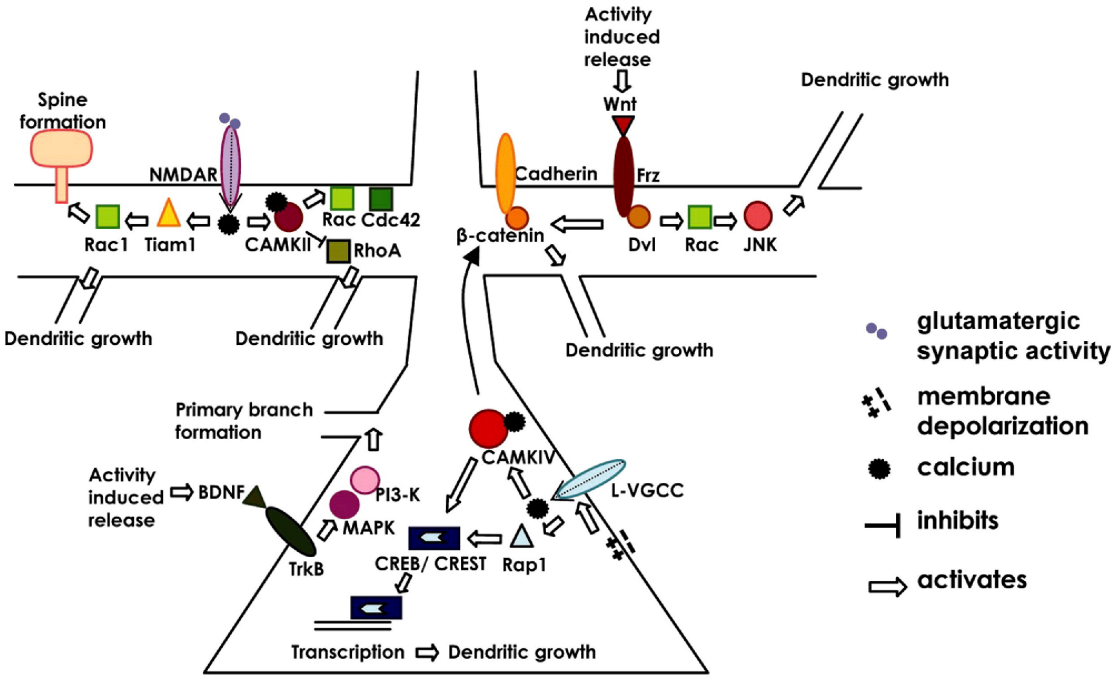

Figure 2.7: Ca^{2+} is an important signal molecule for dendritic development. By neuronal activity Ca^{2+} influx via voltage-gated Ca^{2+} channels and NMDA receptors, as well as release from internal stores is induced. Local Ca^{2+} signals act via Rho family proteins to regulate dendritic branch dynamics and stability, while global Ca^{2+} signals recruit transcriptional mechanisms to regulate dendritic growth. Figure and legend modified from Konur and Ghosh 2005

2.4 Dendritic backpropagation of action potentials

Action potentials in adolescent and mature CA1 pyramidal cells do not only invade the axon, but also elicit backpropagating action potentials (bAP) into the dendritic tree which are dependent on voltage gated sodium channels (Spruston et al. 1995; Stuart et al. 1997; Waters, Schaefer, and Sakmann 2005) in vitro and in vivo (Waters and Helmchen 2004). The depolarization due to the bAP also opens dendritic voltage gated Ca^{2+} channels (Magee and Johnston 1997), Fig. 2.8.

Backpropagation of action potentials is a general principle among different groups of excitatory and inhibitory neurons. Active dendritic backpropagation of APs is also found (Hammond 2008) in pyramidal neurons of neocortex (Stuart and Sakmann 1994; Stuart, Schiller, and Sakmann 1997), in dopaminergic neurons of the substantia nigra pars compacta (Häusser et al. 1995), in Purkinje cells (Stuart and Häusser 1994), in granule cells (Stocca, Schmidt-Hieber, and Bischofberger 2008) and also in thalamic interneurons (Casale and McCormick 2011), in parvalbumin-positive basket cells (Chiovini et al. 2010, in CCK-positive basket cells (Evstratova, Chamberland, and Topolnik 2011).

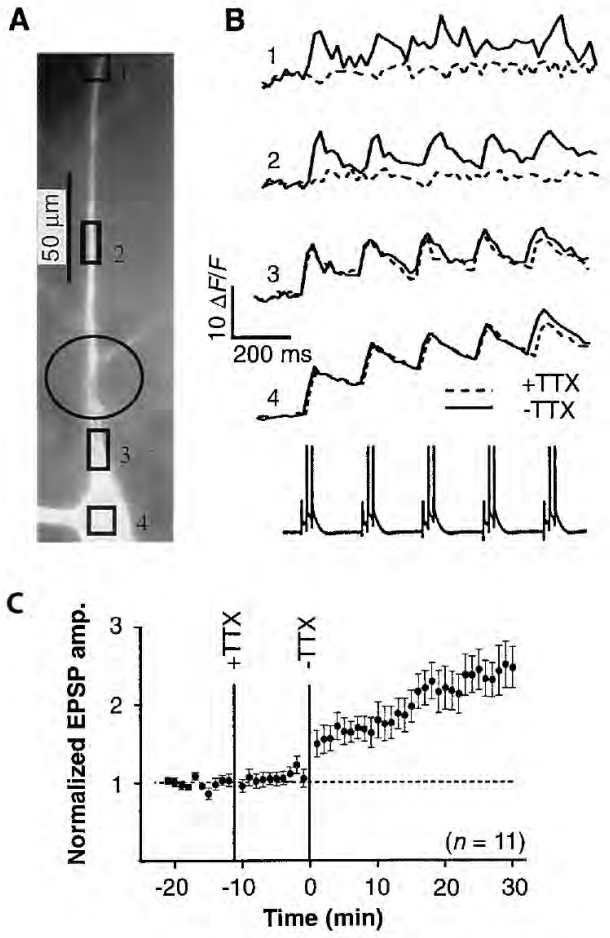

Figure 2.8: Dendritic action potentials are required for induction of synaptic plasticity. **A** Fura-2-filled CA1 pyramidal neuron with somatic electrode of 5- to 10-week-old rat. The approximate area of TTX application is shown by the oval. **B** Superimposed optical recordings from regions of the neuron delimited by boxes in (A). Traces are from progressively more proximal regions moving down the column in (B). Dashed lines are the average $\frac{\Delta F}{F}$ during the pairing protocol given along with a transient application of 10 µM TTX to the dendrite. Solid lines are the average $\frac{\Delta F}{F}$ during the pairing protocol given without TTX application ($\sim$ 11 min later). The increase in $[Ca^{2+}]_i$ is similar in regions of the neuron proximal to the TTX application and is significantly reduced in those regions distal to the TTX application site. *Lower trace*: Somatic voltage during paired train. **C**: Grouped data showing normalized EPSP amplitude after paired stimulation with and without TTX application. Figure and legend from Magee and Johnston 1997.

2.5 Age-dependency of Ca^{2+} extrusion mechanisms

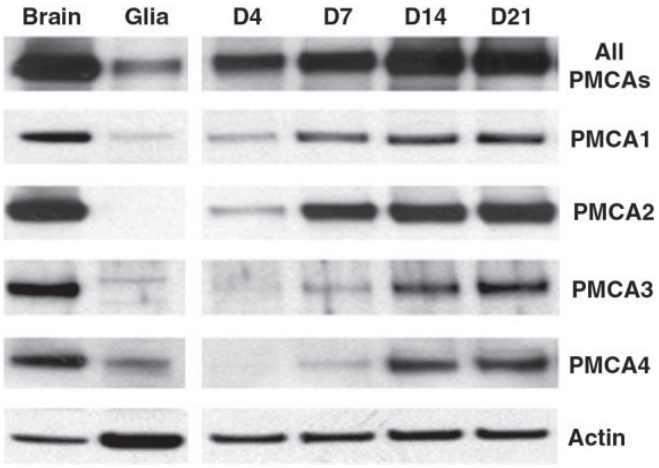

Figure 2.9: Expression of PMCA isoform proteins during maturation of hippocampal neurons in vitro. Total cell lysates were prepared from hippocampal neurons cultured for 4, 7, 14, and 21 days, as well as from total rat brain and 21-day glial cultures as indicated on top of each lane. Figure and legend from Kip et al. 2006

There are several mechanisms how the Ca^{2+} which entered the dendrite after activity is removed from the cytosol, called Ca^{2+} clearance or Ca^{2+} extrusion. Plasma-membrane-ATPases (PMCAs) (Carafoli 1992) which are found in various isoforms pump Ca^{2+} into extracellular space. Compared to Na^{+}/Ca^{2+} exchangers, PMCAs have a 10-fold higher affinity for Ca^{2+}, but a more that 10 times lower transport rate (Blaustein and Lederer 1999).

In addition, Ca^{2+} can be taken up into internal stores (endoplasmatic reticulum) via SERCA pumps (Mainen, Malinow, and Svoboda 1999; Majewska, Tashiro, and Yuste 2000; Sabatini, Oertner, and Svoboda 2002) or into mitochondria (Patterson, Sneyd, and Friel 2007).

The extrusion mechanisms are regulated with age. The development of different Ca^{2+} pumps and transporters was studied using immunocytochemistry, RNA or protein expression. PMCAs are upregulated with age (Fig. 2.9). The isoforms PMCA1, PMCA3 and PMCA4 are gradually upregulated from D4, D7, D14 to D21. The isoform PMCA2 seems to reach mature-like expression already at D7.

In acute slices from rats Jensen, Buckby, and Empson 2004 also found a massive up-regulation of PMCA1-4 but were not able to detect PMCA1 and PMCA2 proteins at P7. For PMCA1 and PMCA2 Jensen, Buckby, and Empson 2004 found a relatively linear up-regulation between P10 and P28. PMCA3 and PMCA4 reached a plateau at P14.

The Western blots results of Kip et al. 2006 and Jensen, Buckby, and Empson 2004 are consistent for PMCA3 and PMCA4. For PMCA1 and PMCA2 there might be a discrepancy between primary hippocampal culture and acute slices.

NCX1, NCX2 and NCX3 appear to be already strongly expressed at D7 and mRNA levels are only slightly increased during next 1-2 weeks (Kip et al. 2006).

Taken together, many different calcium transport systems are expressed early on (∼P7), but are substantially upregulated during the first 2-3 weeks of postnatal development. However, to my knowledge, no functional studies have been performed to address calcium clearance and extrusion in developing CA1 pyramidal cells.

2.6 The aims of this work

In this thesis, I want to address changes in dendritic Ca^{2+} signaling with regard to postnatal development.

To compare developmental regulations, I took two age groups: one week old neonatal rats which are quite immature but their pyramidal cells do not have giant depolarizing potentials any longer and on the other hand four weeks old rats, which are the youngest age at which in vivo mature like properties are found in the hippocampal formation.

I asked the following questions: Nothing was known about dendritic backpropagation in one week old rats. So, is there already active backpropagation as reported for older animals? How do the Ca^{2+} signals look like? Tiny because the Ca^{2+} channel density is still low or large because the dendrite is still lacking molecules which can buffer and therefore reduce the free Ca^{2+} concentration? How do the young neurons handle Ca^{2+} with more than one backpropagating action potential: Is there an activity-dependent modulation of Ca^{2+}-influx or Ca^{2+}-extrusion? Or in other words: Is calcium signalling linearly or non-linearly dependent on AP firing activity? These questions are important for calcium-dependent synaptic and dendritic plasticity as well as for excitotoxicity.

We want to address these questions using high and low affinity Ca^{2+} indicators.

3 Materials and Methods

3.1 Slice preparation

Wistar rats aged 5 to 37 days were kept in an oxygenated chamber for 10 min and then from the age of 3 weeks on anaesthetized with isoflurane (Forene, Abbott; 4-5%) added to the pure oxygen flow via an isofluran vaporator (Drägerwerk AG) and then decapitated, in accordance with German and Swiss guidelines. The dissection of the brain and the subsequent cutting were performed in ice-cold solution (in mM: NaCl 87, $NaHCO_3$ 25, KCl 2.5, NaH_2PO_4 1.25, Glucose 10, Sucrose 75, $MgCl_2$ 7, CaCl 0.5), this solution was also used for storage at room temperature. For 2 weeks old rats and younger usual saline (in mM: NaCl 125, $NaHCO_3$ 25, Glucose 25, KCl 2.5, NaH_2PO_4 1.25, $MgCl_2$ 1, $CaCl_2$ 2) was used for cutting and storage, and for all ages used for recordings, equilibrated with 95% O_2 / 5% CO_2. From the hippocampus transverse 350-µm-thick slices were cut using a Leica VT 1200 slicer. Differing from Bischofberger et al. 2006, the β-angle ('magic cut') was 0° in the case of one week and four weeks old rats, compared to the usual 10-20° for 2 to 3 weeks old rats. Slices were then incubated at 35°C for 30 min.

3.2 Electrophysiology

CA1 pyramidal neurons were identified using infrared differential interference contrast (IR-DIC) video microscopy, preferably in the stratum pyramidale directly neighbouring stratum radiatum with visible apical dendrites. Patch pipettes (4–7 MΩ) were pulled from thick-walled borosilicate glass (outer diameter, 2.0 mm; inner diameter, 1.0 mm) and filled with a K-Gluconate based internal solution containing in mM: K-Gluconate 120-135, KCl 20, $MgCl_2$ 4, Na_2-ATP 2-4, Na-GTP 0.3, Hepes 10, Na_2-phosphocreatine 2, ascorbic acid 0-2, 100-200 µM Fura-FF or 50-200 µM Fura-2, 0.2 % biocytin, filtered before use (Minisart RC4, Membrane 0.2 µm). With the help of K-Gluconate osmolarity was adjusted to 292-313 mOsmol/kg, using the lower range in younger animals, and the pH was adjusted to 7.3 at room temperature, which leads to pH of 7.2 at 33°C.

Whole-cell mode was established, using a Multiclamp 700A amplifier (Molecular Devices, Palo Alto, CA, USA), filtered at 10 kHz and digitized at 20 kHz with a Power1401 interface (Cambridge Electronic Design, Cambridge, UK). For acqui-

sition and commands the custom software FPulse 3.33 (U. Fröbe, University of Freiburg, Germany) was used under Igor 6.21 (WaveMetrics, Lake Oswego, OR, USA). Statistical analysis was performed using GraphPad Prism 5.
The neurons chosen in this study had a resting membrane potential between -75 to -65 mV, for one week old rats -70 to -60 mV, and generated overshooting APs during injection of depolarizing current. Voltage was not corrected for liquid junction potential. The membrane potential was adjusted to about -70 mV throughout the experiment by small depolarizing or hyperpolarizing current injection.
Cells were filled at least 15 min in voltage clamp to monitor stable pipette series resistance ($R_S < 15\text{M}\Omega$). Subsequently, backpropagating action potentials were elicited in current-clamp mode via current injections of 2-ms-duration with an amplitude in the range of ∼0.5-2.5 nA to reliably evoke action potentials. Series resistance and pipette capacitance were compensated. Recordings were made at 33±1°C.
To examine contribution of voltage gated sodium channels to dendritic backpropagation, action potential firing was blocked with 1 µM of TTX (Alomone Labs). Mock action potentials were generated by adjusting the amplitude of 2-ms current pulses until the peak amplitude of the passive somatic voltage response (mock action potentials) was similar to the previously measured AP amplitude.

3.3 Fluorescent measurements

For ratiometric Ca^{2+} imaging the Ca^{2+}-sensitive fluorescent dyes Fura-FF (100-200 µM) or different concentrations of Fura-2 (50, 100 or 200 µM; Invitrogen, Eugene, OR) of previously frozen (-20°C) aliqots (dissolved in water) were added to the pipette solution. The excitation light source (Polychrome V, TILL Photonics, Munich, Germany) was coupled to the epifluorescent port of the microscope via fiber optics (Zeiss Examiner, equipped with 63x/NA1.0 water immersion objective). To minimize bleaching, the light intensity was reduced to 5-10 % by neutral density filters. The filter combination for fluorescence excitation and emission comprised a beam splitter (BSP400) and an emission filter (BP430-630) from AHF Analysentechnik (Tübingen, Germany).
The fluorescence was measured with a Sensicam CCD camera (TILL Photonics Munich, Germany). Images were obtained with 8x32 binning at a repetition rate of 100 Hz using TillVision 4.0. Fluorescence was measured in dendritic regions of interest (typical size 5 x 10 µm, ROI) along the apical dendrite of the CA1 pyramidal cells at a distance of ∼25 µm (proximal) or ∼100 µm (stratum radiatum) from center of soma. The fluorescence signals were corrected for background, which was obtained from neighboring ROIs but shifted by ∼10 to 15 µm with respect to the original ROI, avoiding the presence of dendritic processes (Normann et al. 2000;

Aponte, Bischofberger, and Jonas 2008).

To convert the fluorescence signals into Ca^{2+} concentrations, we used the isosbestic ratioing method (Normann et al. 2000). The action potential-induced fluorescence change was recorded at an excitation wavelength of 380 nm for a duration of about 2-8s. The isosbestic fluorescence was measured immediately before and after these sweeps for about 100-150 ms, respectively, using an excitation wavelength of 357 nm (the Ca^{2+}-insensitive wavelength in our experiments).
Using a self-written macro in TillVision, fluorescence traces of the dendritic region of interest (ROI) for 380 nm (ROI_{den}^{380}), the background region of interest for 380 nm (ROI_{bg}^{380}) and the already background-subtracted and linearly interpolated 357 nm illumination were generated.

3.3.1 Stray-light factor method

We developed a new method to diminish noise on the calcium traces without distorting fast Ca^{2+} transients as it is the usual side effect of conventional box averaging.

The background fluorescence signal usually contained some stray light from the dendritic fluorescence. The stray-light factor f was estimated by calculating the ratio of the peak amplitude of the AP-induced reduction of fluorescence in the background ROI and the dendritic ROI, a typical value in our experiments was $f = 0.4$. As the fluorescence of our ROIs is the sum of a Ca^{2+}-dependent Fura-2 signal F_{raw}^{380} and a Ca^{2+}-independent background signal Bg^{380}, we assume:

$$ROI_{den}^{380} = F_{raw}^{380} + Bg^{380} \tag{3.1}$$

$$ROI_{bg}^{380} = f \cdot F_{raw}^{380} + Bg^{380} \tag{3.2}$$

Eliminating F_{raw}^{380} from equations 3.1 and 3.2 gives the Fura independent background signal Bg^{380}:

$$Bg^{380} = \frac{ROI_{bg}^{380} - f \cdot ROI_{den}^{380}}{1 - f} \tag{3.3}$$

which did not show any AP-induced reduction in fluorescence intensity anymore. Bg^{380} makes up for a large part of the total fluorescence signal, ~90%. Bg^{380} was low-pass filtered by box-averaging (~20-40 pixels) and the smoothed version was called $\widehat{Bg}^{380}$. In our experiments it was not possible to interpolate Bg^{380} linearly. Then the version of F_{raw}^{380} with improved signal-to-noise ratio is (equation 3.1):

$$\widehat{F}_{raw}^{380} = ROI_{den}^{380} - \widehat{Bg}^{380} \tag{3.4}$$

The 360 nm fluorescence signal is already smooth, as it it a linear interpolation. Analog to equation 3.1 and 3.2 one gets:

$$F_{raw}^{357} = \frac{ROI_{dendrite}^{357} - ROI_{bg}^{357}}{1 - f} \tag{3.5}$$

The usual ratio R of both fluorescences is thus given by:

$$R = \frac{F_{raw}^{357}}{\widehat{F}_{raw}^{380}} \tag{3.6}$$

3.4 Calibration of ratiometric Ca^{2+} measurements

The ratio of the background corrected fluorescence signals (equation 3.6) was calculated and converted into the Ca^{2+} concentration using the equation (Grynkiewicz, Poenie, and Tsien 1985):

$$[Ca^{2+}] = K_{eff} \cdot \frac{R - R_{min}}{R_{max} - R} \tag{3.7}$$

with $K_{\text{eff}} = K_d \frac{R_{\max}}{R_{\min}}$ where K_d is the dissociation constant of Fura, $R_{\min}$ the ratio in Ca^{2+}-free solution and $R_{\max}$ the ratio when Fura is completely saturated with Ca^{2+}. $R_{\min}$ and $R_{\max}$ were determined with internal solutions containing either 10 mM EGTA or 10 mM $CaCl_2$. Using these solutions we obtained ratio values for Fura-2 of $R_{\min} = 0.44 \pm 0.01$ (n=5) and $R_{\max} = 3.26 \pm 0.04$ (n=5). The corresponding values for Fura-FF were estimated as $R_{\min} = 0.40 \pm 0.01$ (n=4) and $R_{\max} = 3.20 \pm 0.05$ (n=6). The dissociation constant was assumed to be $K_d = 286$ nM and $K_d = 4.18$ µM for Fura-2 and Fura-FF, respectively (Helmchen, Imoto, and Sakmann 1996; Aponte, Bischofberger, and Jonas 2008). The resting Ca^{2+} concentration obtained with 50-200 µM Fura-2 and the standard internal solution was on average 53 ± 7 nM (n=39) similar to what was reported for CA1 pyramidal neurons (Helmchen, Imoto, and Sakmann 1996).

3.5 Data analysis

Calcium traces were analyzed using custom programs running under Igor 6. To optimize signal-to-noise ratio, 10 to 20 alternating or subsequent sweeps were averaged, low-pass filtered using box-averaging (3 pixels), in addition smoothed with our stray-light factor method (3.3.1) and then the $\frac{F_{357}}{F_{380}}$ ratio was calculated and converted into Ca^{2+} (equation 3.7).

The exponential decay of the Ca^{2+} concentration was either fitted with a monoexponential function, or after theta-burst stimulation, with the sum of two exponentials (i.e. by a biexponential function), and the amplitude-weighted time

constant τ_w was calculated (Aponte, Bischofberger, and Jonas 2008), i.e.

$$\tau_w = \tau_{fast} \cdot \frac{A_{fast}}{A_{fast} + A_{slow}} + \tau_{slow} \cdot \frac{A_{slow}}{A_{fast} + A_{slow}} \tag{3.8}$$

where τ_{fast} and A_{fast} and τ_{slow} and A_{slow} are the decay time constant and the amplitude for each of the two exponentials. The integral remains unchanged, i.e.

$$A_{fast} \cdot \tau_{fast} + A_{slow} \cdot \tau_{slow} = (A_{fast} + A_{slow}) \cdot \tau_w \tag{3.9}$$

3.6 Linear compartment model

To analyze dendritic Ca^{2+} buffering, a single-compartment model was used assuming that influx and equilibration with intracellular Ca^{2+} buffers is fast compared to a linear extrusion mechanism γ as previously described (Helmchen, Imoto, and Sakmann 1996; Aponte, Bischofberger, and Jonas 2008; Helmchen and Konnerth 2011).

Subsections 3.6.1, 3.6.2, 3.6.3, 3.6.4 and 3.6.6 are well-known and based on Helmchen and Konnerth 2011 and Helmchen, Imoto, and Sakmann 1996. Additionally, subsections 3.6.1 and 3.6.2 are partly based on Pohle 2007.

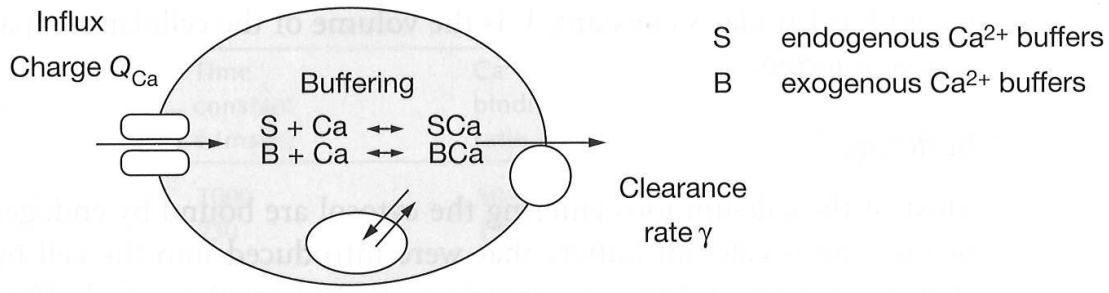

Figure 3.1: The one-compartment model: Calcium flows into the cell with the charge Q_{Ca}. It will be partially bound to intrinsic buffers S and to the exogenous calcium indicator B. The increased calcium is removed from the cytosol with an extrusion rate γ. The analyzed dendritic segment has a diameter of about 2 µm and a typical length of 10 µm and is considered as one compartment in which diffusion is on a faster timescale than the decay of the calcium transient. (Fig. from Helmchen and Konnerth 2011)

3.6.1 Influx

Mainly through voltage gated Ca^{2+} channels, a certain charge Q_{Ca} of Ca^{2+} ions enters the dendrite, when the dendritic membrane is depolarized in our experiments

by one backpropagating action potential. From Faraday's law of electrolysis, given the charge Q_{Ca}, the amount of substance n, the valency number of ions z of the substance ($z = 2$ for calcium) and the Faraday constant F, it follows:

$$Q_{\mathrm{Ca}} = n \cdot z \cdot F = \Delta[\mathrm{Ca}^{2+}]_{\mathrm{T}} \cdot V \cdot z \cdot F \tag{3.10}$$

where V is the volume of the dendritic compartment and $\Delta[\mathrm{Ca}^{2+}]_{\mathrm{T}}$ the change in total calcium concentration (free and bound to buffer).

An important assumption of the one-compartment model is that the inflow of the total calcium $\Delta[\mathrm{Ca}^{2+}]_{\mathrm{T}}$ is much faster than the following decay of the calcium transient. Then it is possible to assume $[\mathrm{Ca}^{2+}]_{\mathrm{T}} \cdot \delta(t)$ as the calcium inflow at $t = 0$. $\delta(t)$ is the Dirac delta distribution. Then the calcium inflow j_{in} is:

$$j_{\mathrm{in}} = \Delta[\mathrm{Ca}^{2+}]_{\mathrm{T}} \cdot \delta(t) = \frac{Q_{\mathrm{Ca}}}{2FV} \cdot \delta(t) \tag{3.11}$$

3.6.2 Ca^{2+} buffering

When measuring the Ca^{2+} concentration, the Ca^{2+} indicator adds additional, exogenous buffer B to the endogenous buffer S of the dendrite, thus the free calcium is partially bound (=buffered) via:

$$[S] + [\mathrm{Ca}^{2+}]_i \leftrightarrow [S\mathrm{Ca}] \tag{3.12}$$

and

$$[B] + [\mathrm{Ca}^{2+}]_i \leftrightarrow [B\mathrm{Ca}] \tag{3.13}$$

$[B]$ is the concentration of the unbound exogenous buffer, $[\mathrm{Ca}^{2+}]_{\mathrm{i}}$ the concentration of the unbound calcium and $[B\mathrm{Ca}]$ the concentration of the exogenous buffer bound to calcium. With $[B]_{\mathrm{T}}$ as the total exogenous buffer concentration (Fura):

$$[B] + [B\mathrm{Ca}] = [B]_{\mathrm{T}} \tag{3.14}$$

The dissociation constant of equation 3.13 is given by

$$K_{\mathrm{d}} = \frac{[\mathrm{Ca}^{2+}]_{\mathrm{i}} \cdot [B]}{[B\mathrm{Ca}]} \tag{3.15}$$

From equation 3.14 and 3.15 it follows:

$$\frac{[BCa]}{[B]_{\mathrm{T}}} = \frac{[\mathrm{Ca}^{2+}]_i}{K_d + [\mathrm{Ca}^{2+}]_i} \tag{3.16}$$

and

$$[BCa] = \frac{[\mathrm{Ca}^{2+}]_i [B_T]}{K_d + [\mathrm{Ca}^{2+}]_i} \tag{3.17}$$

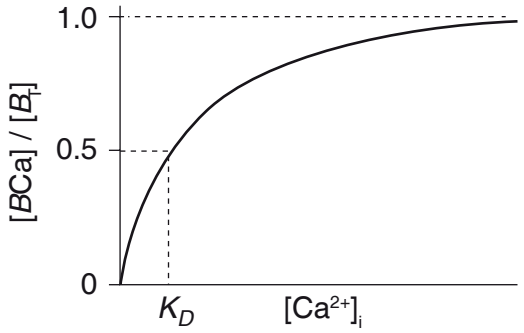

Figure 3.2: Relationship between the concentrations of free Ca^{2+} and Ca^{2+}-bound buffer. The non-linear curve implies that κ_B decreases when Ca^{2+} increases. For a free Ca^{2+} concentration at the same level as the K_d of the Ca^{2+} indicator, $\frac{1}{2}$ of the exogenous buffer is bound. Modified from Higley and Sabatini 2012.

The calcium buffer capacity (also called calcium binding ratio) κ_B is given by (Neher and Augustine 1992):

$$\kappa_B := \frac{\partial[BCa]}{\partial[\mathrm{Ca}^{2+}]_i} \tag{3.18}$$

With the help of equation 3.17 and using the quotient rule for derivatives for equation 3.18 one gets:

$$\kappa_B = \frac{[B_T] \cdot K_d}{(K_d + [\mathrm{Ca}^{2+}]_i)^2} \approx \frac{[B_T] \cdot K_d}{(K_d + [\mathrm{Ca}^{2+}]_{\mathrm{rest}})(K_d + [\mathrm{Ca}^{2+}]_{\mathrm{rest}} + \Delta[\mathrm{Ca}^{2+}]_i)} \tag{3.19}$$

The right approximation is made for approximating the buffer capacity of the Ca^{2+} indicator for relatively small $\Delta[\mathrm{Ca}^{2+}]_i$ transients starting at resting Ca^{2+} concentration $[\mathrm{Ca}^{2+}]_{\mathrm{rest}}$.

If the concentration of free calcium is much lower than the dissociation constant K_d, one can approximate equation 3.19

$$\kappa_B \approx \frac{[B_T]}{K_d} \tag{3.20}$$

This equation is valid in the case of a low affinity calcium indicator like Fura FF, but not for a high affinity calcium indicator like Fura 2.

In the same way as in equation 3.18 one defines the calcium buffer capacity (calcium binding ratio) κ_S for the endogenous calcium buffer in the dendrite:

$$\kappa_S := \frac{\partial[SCa]}{\partial[\mathrm{Ca}^{2+}]_i} \tag{3.21}$$

κ_S gives a measure of the calcium buffer molecules. For example a value of κ_S=100 means that 100 Ca^{2+} molecules are bound and only one is free. Usually the buffer capacity is approximated linearly (c.f. Fig. 3.2).

3.6.3 Ca^{2+} clearance from the cytosol

The Ca^{2+} extrusion rate is assumed to be proportional to the increase of the free calcium from the resting calcium concentration – with the proportionality factor γ, the extrusion rate. Thus, extrusion can be expressed as:

$$j_{\text{out}} = -\gamma \cdot \Delta[\text{Ca}^{2+}]_i = -\gamma \cdot ([\text{Ca}^{2+}]_i - [\text{Ca}^{2+}]_{\text{rest}}) \tag{3.22}$$

3.6.4 Calcium dynamics

Influx, buffering and extrusion is described by:

$$\frac{\mathrm{d}[\text{Ca}^{2+}]_T}{\mathrm{d}t} = j_{\text{in}} + j_{\text{out}} \tag{3.23}$$

with $[Ca^{2+}]_T$ the total calcium concentration in the cytosol.
Thus it follows for a Ca^{2+} influx at $t = 0$:

$$\frac{\mathrm{d}[\text{Ca}^{2+}]_i}{\mathrm{d}t}(1 + \kappa_S + \kappa_B) = \Delta[\text{Ca}^{2+}]_T \delta(t) - \gamma \Delta[\text{Ca}^{2+}]_i \tag{3.24}$$

as described by Helmchen, Imoto, and Sakmann 1996.

3.6.5 Solution of equation for one-compartment model

Now I derive the solution of the one-compartment model. On the one hand the solution is well known and derived in literature (e.g. Helmchen, Imoto, and Sakmann 1996), on the other hand having in mind that the one-compartment model is very simplistic and one probably wants to modify it sometime, I apply a general solution method for differential equations, namely Laplace transform (c.f. Gustafson and Wilcox 1998).

With this general solution method, it would be possible to expand the equation 3.24 and for example to consider extrusion mechanisms consisting of several components resulting in an extrusion rate which is not constant over time.

Furthermore, one would not be restricted to assume a δ-like, fast Ca^{2+} influx.

I start with the well-known equation for the one-compartment model (equation 3.24):

$$(1 + \kappa_S + \kappa_B)\frac{\mathrm{d}[\text{Ca}^{2+}]_{\text{i}}}{\mathrm{d}t} + \gamma \Delta[\text{Ca}^{2+}]_{\text{i}} = \Delta[\text{Ca}^{2+}]_{\text{T}} \delta(t) \tag{3.25}$$

Then one applies the Laplace transform $\mathcal{L}$ across the equation and exploits $\mathcal{L}(\delta(t)) = 1$:

$$(1 + \kappa_S + \kappa_B)\mathcal{L}(\frac{\mathrm{d}[\mathrm{Ca}^{2+}]_\mathrm{i}}{\mathrm{d}t}) + \gamma\mathcal{L}(\Delta[\mathrm{Ca}^{2+}]_\mathrm{i}) = \Delta[\mathrm{Ca}^{2+}]_\mathrm{T} \tag{3.26}$$

Then I use the derivative rule on $\frac{\mathrm{d}[\mathrm{Ca}^{2+}]_\mathrm{i}}{\mathrm{d}t}$:

$$(1 + \kappa_S + \kappa_B)\left(s\mathcal{L}(\Delta[\mathrm{Ca}^{2+}]_\mathrm{i}) - \Delta[\mathrm{Ca}^{2+}]_\mathrm{i}(0)\right) + \gamma\mathcal{L}(\Delta[\mathrm{Ca}^{2+}]_\mathrm{i}) = \Delta[\mathrm{Ca}^{2+}]_\mathrm{T} \tag{3.27}$$

Now using the initial condition $\Delta[\mathrm{Ca}^{2+}]_\mathrm{i}(0) = 0$:

$$\mathcal{L}(\Delta[\mathrm{Ca}^{2+}]_\mathrm{i}) = \frac{\Delta[\mathrm{Ca}^{2+}]_\mathrm{T}}{(1 + \kappa_S + \kappa_B)s + \gamma} \tag{3.28}$$

$$= \frac{\Delta[\mathrm{Ca}^{2+}]_\mathrm{T}}{1 + \kappa_S + \kappa_B} \cdot \frac{1}{s + \frac{\gamma}{1+\kappa_S+\kappa_B}} \tag{3.29}$$

Knowing $\mathcal{L}(A \exp \frac{-t}{\tau}) = A\frac{1}{s+\frac{1}{\tau}}$ and using Lerch's theorem:

$$\Delta[\mathrm{Ca}^{2+}]_\mathrm{i} = A \cdot \exp \frac{-t}{\tau} \tag{3.30}$$

with the amplitude

$$A = \frac{\Delta[\mathrm{Ca}^{2+}]_\mathrm{T}}{1 + \kappa_S + \kappa_B} \tag{3.31}$$

and the decay time constant τ

$$\tau = \frac{1 + \kappa_S + \kappa_B}{\gamma} \tag{3.32}$$

$\Delta[\mathrm{Ca}^{2+}]_\mathrm{i}$ is the relative Ca^{2+} elevation above resting Ca^{2+} concentration, $[\mathrm{Ca}^{2+}]_\mathrm{rest}$.

3.6.6 Consequences of the one-compartment-model

Equation 3.30 describes the dynamics of Ca^{2+} transients with the following implications (Fig. 3.3):

Doubling the Ca^{2+} influx, doubles the amplitude A, but does not change the decay time constant τ.

A 2-times increase in calcium binding ratio κ_S leads to a reduction of 50% of the amplitude A and a doubling of the decay time constant τ.

A reduction of the extrusion rate γ to 50% leads to a doubling of the decay time constant τ, but leaves A intact.

The endogenous Ca^{2+}-binding ratio κ_S was estimated by competition with the exogenous Ca^{2+} buffers Fura-2 and Fura-FF. Therefore, the peak amplitude of

single AP-evoked transients was estimated by extrapolation of the monoexponential time course to the mid-point of the rising phase as in Helmchen, Imoto, and Sakmann 1996. The inverse amplitude (equation 3.31) of the Ca^{2+} transients was plotted against exogenous Ca^{2+}-binding ratio κ_B, and κ_S as well as the total calcium load $\Delta[Ca^{2+}]_T$ was obtained by linear extrapolation:

$$\frac{1}{A} = \frac{1 + \kappa_B + \kappa_S}{\Delta[Ca^{2+}]_T} \tag{3.33}$$

Furthermore, the decay time constant τ was plotted against κ_B to obtain the Ca^{2+}-extrusion rate γ by linear extrapolation to (equation 3.32):

$$\tau = \frac{1 + \kappa_B + \kappa_S}{\gamma} \tag{3.34}$$

The crossings of the linear regression line with the x-axis in equations 3.33 and 3.34 is $-(\kappa_S + 1)$.

A_0 is the Ca^{2+} amplitude (equation 3.31) unaffected by exogenous buffer capacity (i.e. for κ_B=0). τ_0 is the decay time constant (equation 3.32) unaffected by exogenous buffer capacity (i.e. for κ_B=0).

The integral of $\Delta[Ca^{2+}]_i$ is (Helmchen, Imoto, and Sakmann 1996)

$$A \cdot \tau = \frac{\Delta[Ca^{2+}]_T}{\gamma} \tag{3.35}$$

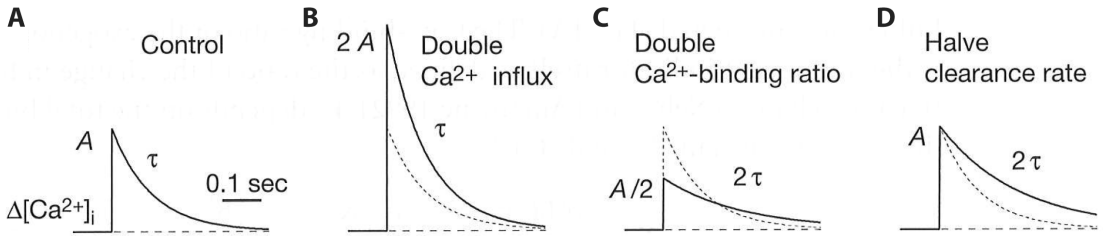

Figure 3.3: Changes in Ca^{2+} transients according to changes in Ca^{2+} influx, κ_S, κ_B and γ: **A**: Ca^{2+} influx induces a monoexponential Ca^{2+} transient as described in equation 3.30. **B**: If Ca^{2+} influx doubles, so does A, but τ remains. **C**: If κ_S or κ_B doubles, A decreases to 50% and τ doubles. **D**: If γ halves, τ doubles, A remains. From Helmchen and Konnerth 2011

3.7 Modelling of linear dendritic Ca^{2+} signaling during short bursts

In order to simulate dendritic Ca^{2+} accumulation we modelled linear summation of AP-evoked Ca^{2+} transients using the amplitude A_1 and the decay time constant τ_1 measured with Fura FF for a single AP. For short bursts of n APs with an interspike interval Δt the peak amplitude A_n was calculated either numerically as the linear sum of single transients:

$$A_n = A_1 \cdot \sum_{i=1}^{n} \exp \frac{-(i-1)\Delta t}{\tau_1} \tag{3.36}$$

or indirectly via geometric progression as:

$$A_n = A_1 \cdot \frac{1-a^n}{1-a}, \text{ with } a := \exp \frac{-\Delta t}{\tau_1} \tag{3.37}$$

similar to what was previously described by Regehr and Tank 1994; Helmchen and Konnerth 2011.

3.8 Modelling of non-linear Ca^{2+} signaling during theta bursts firing

During theta-burst stimulation (TBS_n) brief bursts of n APs (3-10 APs at 100 Hz) were repeated 10 times at a rate of 5 Hz. To model Ca^{2+} accumulation during TBS we had to take into account that the Ca^{2+} influx, and therefore the slope of rise of the individual burst-evoked i^{th} Ca^{2+} transient decreased with time. This was represented by an experimentally obtained normalized rise-time factor $r_i<1$ for $i \geq 2$.

$$\int_{t=0}^{\infty} \Delta[Ca^{2+}]_i dt = n \cdot A_1 \cdot \tau_1 \cdot \sum_{i=1}^{10} r_i \tag{3.38}$$

Furthermore, the time dependent slow-down of the Ca^{2+}-decay time constant was modelled as an exponential transition from single burst decay τ_1 towards the decay time constant measured after the last burst τ_{10}. As a result the integral of the Ca^{2+} signal calculates as:

$$\int_{t=0}^{\infty} \Delta[Ca^{2+}]_i dt = n \cdot A_1 \cdot \tau_1 \sum_{i=1}^{10} \left(r_i \left(\exp \frac{-(i-1)\Delta t}{T_{\text{TBS}}} + (1 - \exp \frac{-(i-1)\Delta t}{T_{\text{TBS}}}) \frac{\tau_{slow}}{\tau_1} \right) \right) \tag{3.39}$$

with $\Delta t = 0.2$ s and T_{TBS} representing the time constant of the slow-down of the Ca^{2+} extrusion rate measured after the individual burst during the TBS paradigm.

3.9 Statistics

Statistical significance was assessed by two-tailed unpaired t-tests or, as indicated, by non-parametric Mann-Whitney test when Gaussian distribution was not assumed.

3.10 Age binning

One week old rats consisted of P7-P9 and four weeks old rats consisted of P26-P29.

4 Results

4.1 Active dendritic backpropagation in young CA1 pyramidal cells

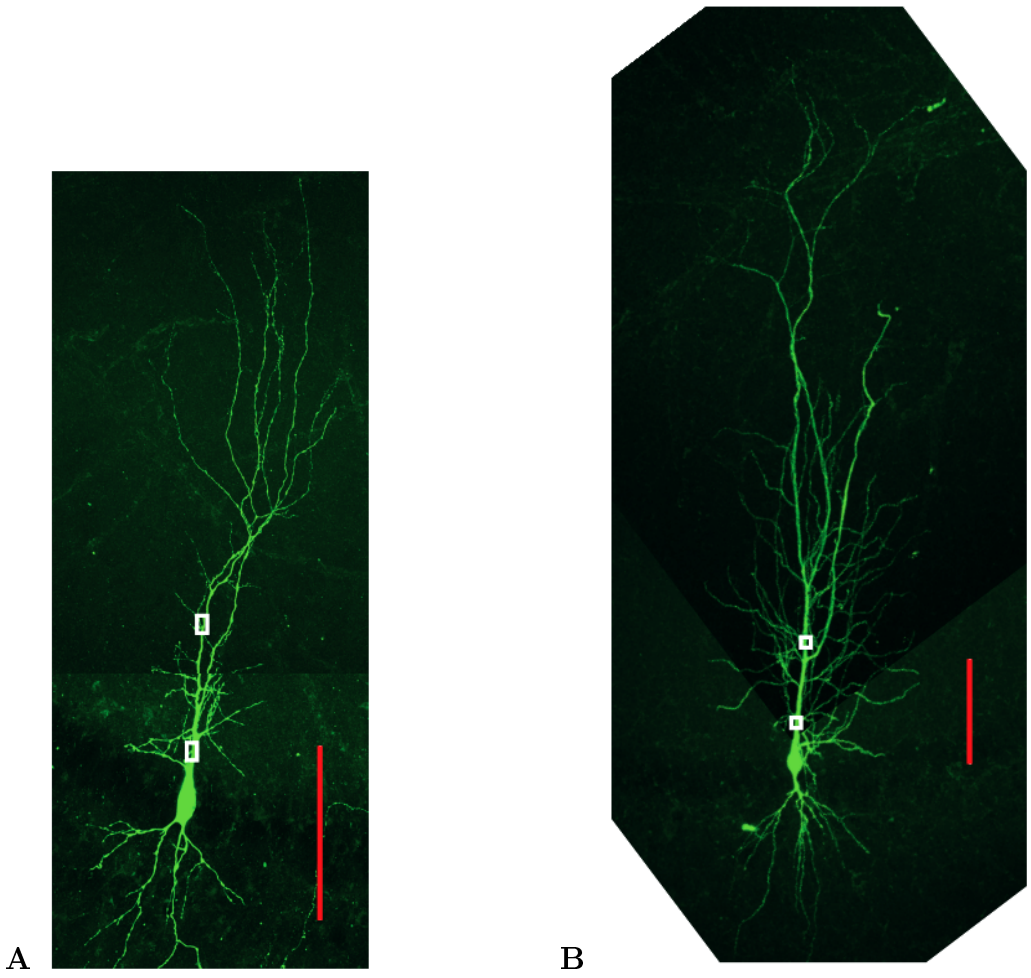

Figure 4.1: **A**: Biocytin filled pyramidal neuron of P7 rat. Red scaling bar represents 100 µm. **B**: Biocytin filled pyramidal neuron of P27 rat. Red scaling bar represents 100 µm. White boxes show control region of interest at 25 µm and second region of interest at 100 µm in stratum radiatum.

To study the postnatal development of action potential (AP)-induced dendritic Ca^{2+} transients in CA1 pyramidal cells, we performed whole-cell patch-clamp recordings and ratiometric Ca^{2+} imaging in acute rat hippocampal brain slices (P5-P37). Using the low-affinity fluorescent Ca^{2+}-indicator Fura-FF and a cooled CCD-camera system, we found large AP-evoked dendritic Ca^{2+} transients already in 1-week-old animals (Fig. 4.2).

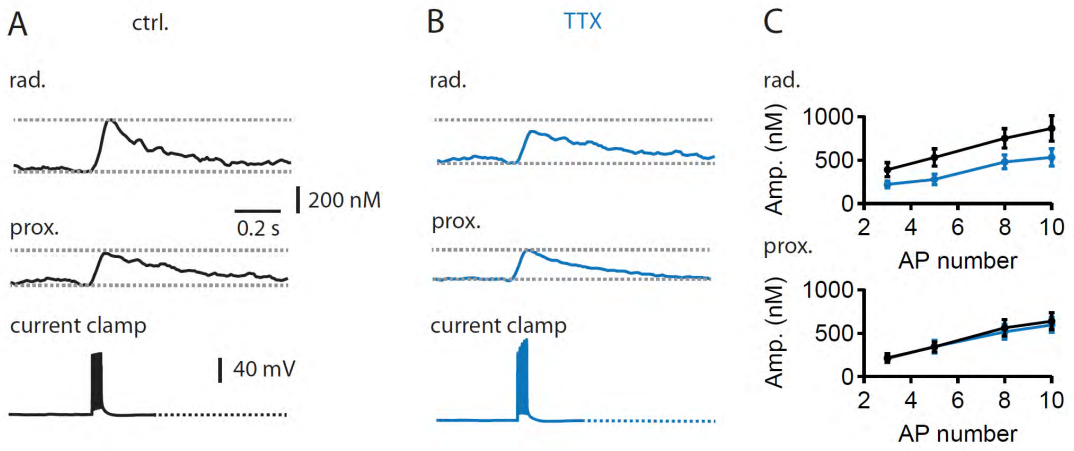

Figure 4.2: **A**: Example traces for P7 rat in Fig. 4.1A using normal saline. *Top*: Ca^{2+} transient of a brief 100 Hz burst of 5 APs in stratum radiatum, 100 µm from mid-soma, *middle*: at the same time the Ca^{2+} transient at 25 µm, very proximal for control, *bottom*: corresponding e-phys traces in current clamp. **B**: Example traces for the same cell as in (A), but after bath-applying 100 µM TTX in saline. **C**: *Top*: Average amplitudes (±SEM) for n=4 one week old rats in control (black) and in 100 µM TTX (blue) at 100 µm from mid-soma. Both traces are significantly different (3 APs: P=0.044 paired, 5 APs: P=0.031 paired, 8 APs: P=0.027 paired, 10 APs: P=0.010 paired). *Bottom*: Average amplitudes (±SEM) in control (black) and with 100 µM TTX (blue) at 25 µm.

A brief burst of 5 APs evoked Ca^{2+} transients in the apical dendrites of 1-week-old pyramidal cells with an amplitude of 342±59 nM and 530±99 nM (n=4) at a distance of 25 µm and 100 µm from soma, respectively (Fig. 4.1A and 4.2AC). Four weeks old rats showed an amplitude of 580±65 nM and 476±66 nM (n=4) at corresponding distances from soma (Fig. 4.1B and 4.3AC). Remarkably, there was no significant difference between 1 week old rats and 4 weeks old rats, at 100 µm (P=0.666). Similar results were obtained with bursts of 3, 5, 8 and 10 APs (Fig. 4.2C and 4.3C, upper panel) in 1-week- (grey) and 4-week-old animals (black).

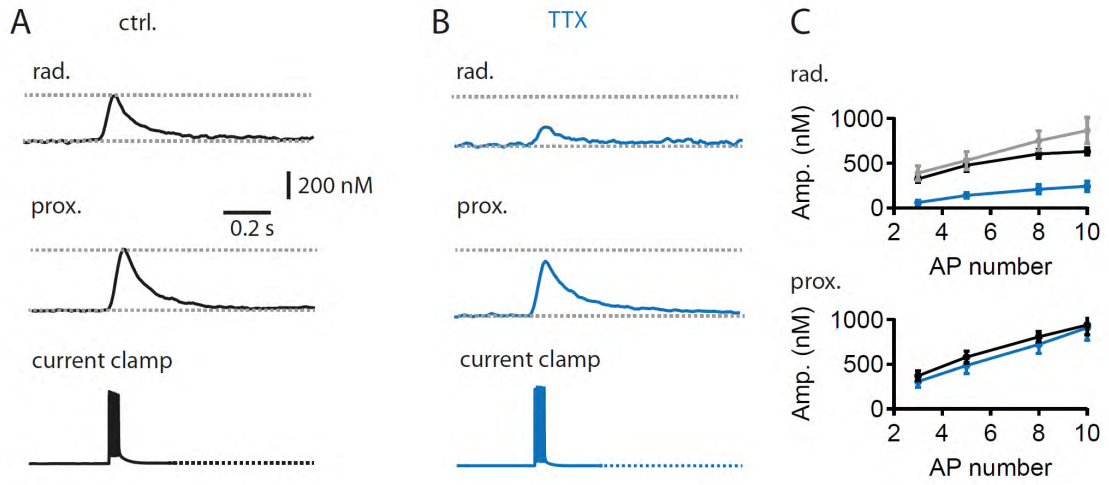

Figure 4.3: **A**: Example traces for P27 rat in Fig. 4.1B using normal saline. *Top*: Ca^{2+} transient of a brief 100 Hz burst of 5 APs in stratum radiatum, 100 µm from mid-soma, *middle*: at the same time the Ca^{2+} transient at 25 µm, very proximal for control, *bottom*: corresponding e-phys traces in current clamp. **B**: Example traces for the same cell as in (A), but after bath-applying 100 µM TTX in saline. **C**: *Top*: Average amplitudes (± SEM) for n=4 four weeks old rats in control (black) and in 100 µM TTX (blue) at 100 µm from mid-soma. Both traces are significantly different (3 APs: P=0.020 paired, 5 APs: P=0.022 paired, 8 APs: P=0.006 paired, 10 APs: P=0.025 paired). *Bottom*: Average amplitudes (±SEM) in control (black) and with 100 µM TTX (blue) at 25 µm.

To analyze the contribution of voltage-gated sodium channels to dendritic back-propagation we bath-applied 1 µM TTX and generated brief bursts of 3-10 mock action potentials with a similar amplitude (115.9±2,8 mV, average for 5APs) as voltage gated sodium channel dependent APs (103.5±1.4 mV, average over 5 APs, n=4 cells, Fig. 4.4) in young as well as in mature pyramidal cells (115.2±2.7 mV versus 104.8±1.7 mV, average over 5 APs, n=4 cells). There was a certain increase in the mock action potential height during the burst, probably leading to a slight underestimation of the role of voltage gated sodium channels.

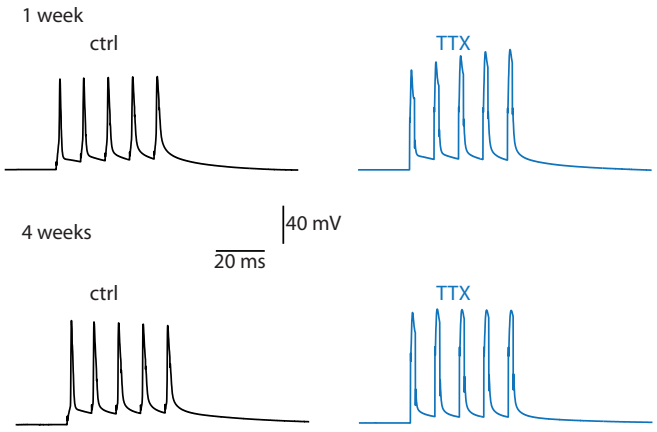

Figure 4.4: `Action potentials vs mock action potentials`

The mock APs generated similar Ca^{2+} transients in proximal dendrites (∼25 µm) in young (Fig. 4.2BC) as well as in mature pyramidal cells (Fig. 4.3BC). By contrast, in the middle of stratum radiatum (∼100 µm from mid-soma), the amplitude of Ca^{2+} transients was significantly reduced at both age groups for 3-10 APs, with a bursts of 5 APs to 50% (n=4, P=0.031, paired) and 30% (n=4, P=0.022, paired) of control at 1 and 4 weeks, indicating active dendritic backpropagation.

We further plotted the amplitude of backpropagation-induced dendritic Ca^{2+} transients (burst of 5 APs) versus the age of the animals (Fig. 4.5AC), showing that dendritic Ca^{2+} transients rapidly increases after P5. Fitting an exponential function (without x-offset) indicates that the amplitude is already 81% at P8 and 99% at P14 relative to 4-week-old animals at 100 µm distance. Similarly, the decay time constant of Ca^{2+} transients was slower in young animals, but rapidly decreased to 175% and 107% at P8 and P14, respectively.

These data indicate that AP are actively backpropagated into apical dendrites of immature CA1 pyramidal cells, generating large Ca^{2+} transients with mature-like amplitude already at 1 week (P8) and mature-like decay already at 2 weeks.

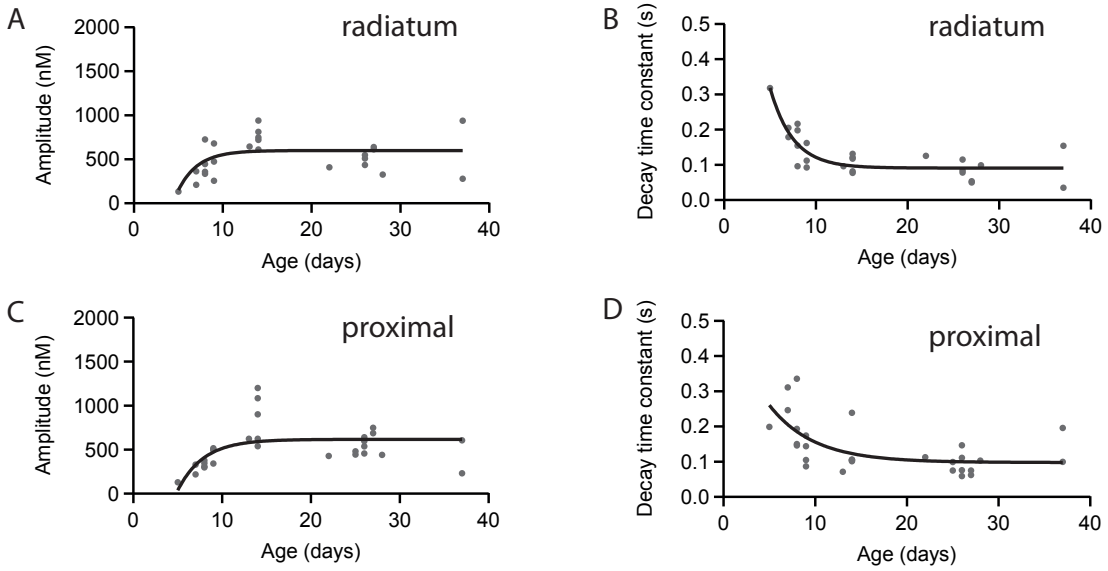

Figure 4.5: Rapid postnatal development of dendritic Ca^{2+} transients. **A**: Circles represent measured Ca^{2+} amplitudes in stratum radiatum at 100 µm for brief bursts of 5 APs at 100 Hz, plotted against age of the rats. Data points are fitted parameter-free (with x_0=0) by a monoexponential function (black trace). **B**: Circles represent measured Ca^{2+} monoexponential decay time constants for data from (A) in stratum radiatum at 100 µm for brief bursts of 5 APs at 100 Hz, plotted against age of the rats. Data points are fitted parameter-free (with x_0=0) by a monoexponential function (black trace). **C**: Amplitudes as in (A), but very proximal at 25 µm from mid-soma. **D**: Monoexponential decay time constants of Ca^{2+} transients from (C)

4.2 Postnatal development of Ca^{2+} buffering and extrusion

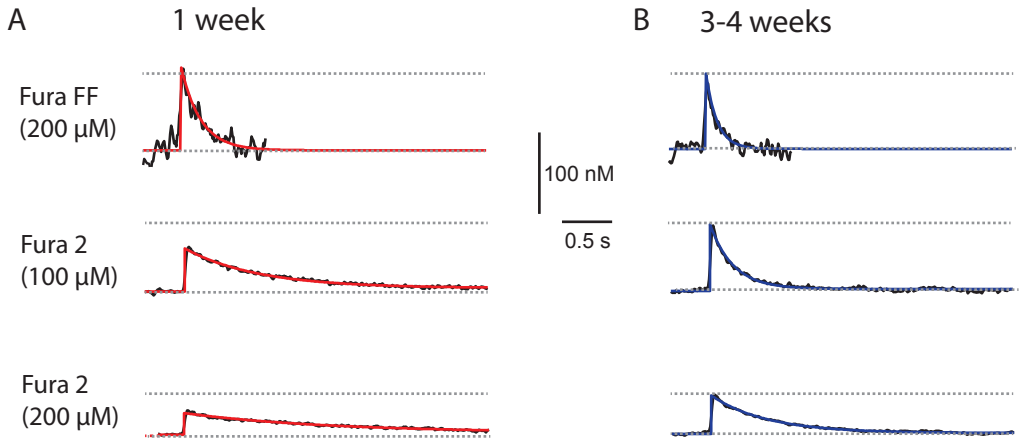

Figure 4.6: **A** Example traces for a one week old rat using Fura-FF and different concentrations of Fura-2. Black traces are the measured Ca^{2+} transients induced by one AP. Red traces are fit by a monoexponential function which is extrapolated to the mid-point of the rising phase. **B** Example traces for a four weeks old rat using Fura-FF and different concentrations of Fura-2. Black traces are the measured Ca^{2+} transients induced by one AP. Blue traces are fit by a monoexponential function which is extrapolated to the mid-point of the rising phase.

The large amplitudes of dendritic Ca^{2+} signals in young animals could be generated by high density of voltage-gated Ca^{2+} channels, slow time course of dendritic APs or reduced dendritic Ca^{2+} buffering in young cells. To understand the underlying mechanisms we compared dendritic Ca^{2+} influx and buffering in 1 and 3-4-week old animals using different concentrations of Fura-2 and Fura-FF to differentially compete with endogenous dendritic Ca^{2+} buffers (Helmchen, Imoto, and Sakmann 1996). As shown in Fig. 4.6, the application of 100 µM Fura 2 significantly reduced the amplitude of Ca^{2+} transients in young and mature cells evoked by single backpropagating APs as compared to Fura-FF. However, the effect of Fura 2 was much larger in the 1-week-old animals (n=23) than at 4 weeks (n=28, 4.7AC). To estimate the total Ca^{2+} influx $\Delta[Ca^{2+}]_T$ and the endogenous Ca^{2+} binding ratio κ_S we plotted the inverse amplitude against the exogenous binding ratio introduced by Fura-2 (Fig. 4.7AC, equation 3.19 and 3.33). Consistent with a linear compartment model we could fit the data from young cells by linear regression (r^2 = 0.60), which revealed $\Delta[Ca^{2+}]_T$ = 10±2 µM and an endogenous binding ratio κ_S = 69±52 from slope and x-axes intercept, respectively (equation 3.33, Table 4.1). By contrast, in mature cells (r^2 = 0.74) calcium load ($\Delta[Ca^{2+}]_T$ = 44±5

µM) as well as the endogenous binding ratio (κ_S = 276±45) were about 4-times larger. As a result, the amplitude of single-AP evoked Ca^{2+} transients revealed by the inverse y-axes intercept was very similar in young (A_0 = 137 nM) and mature cells (A_0 = 160 nM). The extrapolated amplitudes were also similar to the amplitudes directly measured with 100-200 µM Fura-FF in young (A_1 = 108±20 nM, n=6) and mature cells (A_1 = 103±12 nM, n=7), which were not significantly different between the two age groups (P=0.804). These data indicate that there is a large increase of dendritic Ca^{2+} influx during the first 4 weeks of postnatal development. However, this seems to be compensated, by a similar increase in endogenous buffer capacity. As a result the amplitude of Ca^{2+} signals evoked by single APs (Fig. 4.7) or by briefs burst of APs have similar amplitude throughout postnatal development (Fig. 4.3; 4.5).

The decay of the dendritic Ca^{2+} transients could be well fitted by a monoexponential function independent of cell age. Similar to the amplitude analysis, we plotted the decay time constant τ against κ_B. Linear regression (r^2 = 0.81 in 1 week, 0.54 in 3-4 weeks old rats) revealed an about 4.5-times smaller extrusion rate of γ = 337±35 s^{-1} at 1 week versus γ = 1444±263 s^{-1} at 3-4 weeks of age (equation 3.34, table 4.1). Again, due to compensatory increase in κ_S there is only a relatively small but significant decrease in the resulting average decay time constant from τ = 170±9 ms in young towards τ = 93±5 ms at 4 weeks of age, as directly measured with Fura-FF for brief bursts of 1 to 10 APs (n=35 tau values for 1 week, n=33 for 4 weeks, P<0.0001, averaging over all AP numbers for n=5-9 young cells and n=5-7 mature cells, c.f. figure 4.9).

Using these Fura FF decay time constants to calculate the resulting Ca^{2+} extrusion rate via equation 3.32 gives values for extrusion rates for both 1 week old rats as well as 3-4 weeks old rats which are about twice the values calculated from Fig. 4.7BD, namely 635±249 s^{-1} and 3000±597 s^{-1} respectively.

Briefly, mature neurons have a 4.5-times larger Ca^{2+} extrusion rate than young neurons.

In table 4.1 the quantitative values of figure 4.7 are given. κ_S could also be calculated from the τ vs κ_B plot.

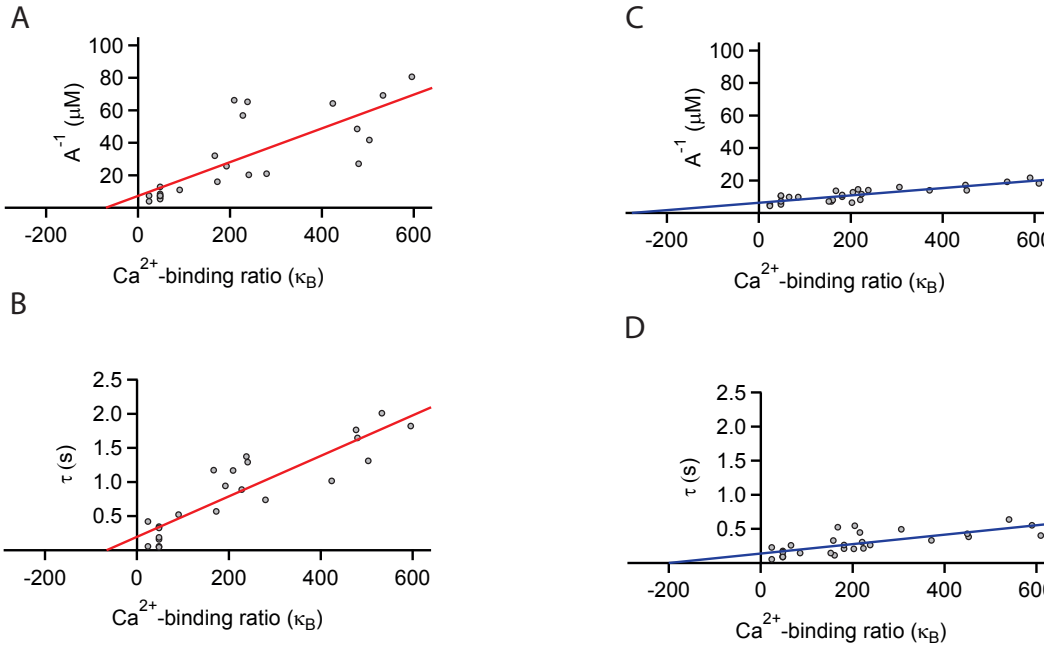

Figure 4.7: Quantification of values for one-compartment-model. **A**: Inverse amplitudes vs κ_B in one week old rats **B**: Decay time constants vs κ_B in one week old rats. **C**: Inverse amplitudes vs κ_B in three to four weeks old rats. **D**: Decay time constants vs κ_B in three to four weeks old rats

	1 week	3-4 weeks
κ_S (from A^{-1})	69 (± 52)	276 (± 45)
κ_S (from τ)	65 (± 31)	200 (± 62)
average κ_S	67	238
$[Ca^{2+}]_T$ [µM]	10 (± 2)	44 (± 5)
A_0 [nM]	137 (± 101)	160 (± 18)
τ_0 [ms]	196 (± 90)	138 (± 35)
γ [1/s]	337 (± 35)	1444 (± 263)

Table 4.1: Results of buffer capacity experiment κ_S is calculated from A^{-1} respectively τ vs κ_B plot. Average κ_S for both methods is given. $[Ca^{2+}]_T$ is calculated from inverse slopes in Fig. 4.7AC and A_0 is the respective crossing with the y-axis. τ_0 is calculated from crossing of linear regression line in 4.7BD with y-axis. γ is inverse slope in Fig. 4.7BD

4.3 Linear summation of Ca^{2+} transients during brief bursts of APs

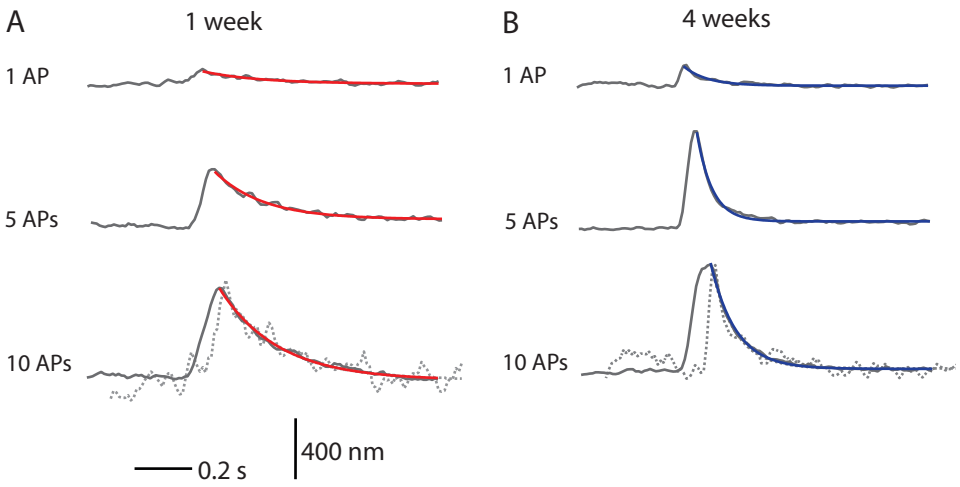

Figure 4.8: Decay rate scales linearly with amplitude of Ca^{2+} transients during brief bursts of APs. **A**: Example traces for one week old rat. Measured Ca^{2+} transients in grey. Decay at the end fitted by a monoexponential function in red. Dashed lines enlarge the measured Ca^{2+} trace of 1 AP to the amplitude size of 10 APs. **B**: Examples traces for a four weeks old rat. Measured Ca^{2+} transients in grey. Decay at the end fitted by a monoexponential function in blue. Dashed lines enlarge the measured Ca^{2+} trace of 1 AP to the amplitude size of 10 APs.

To investigate activity-dependent summation of dendritic Ca^{2+} transients during repetitive AP firing, we first compared the decay of Ca^{2+} transients after single APs with the decay after brief bursts of 3, 5, 8 and 10 APs using Fura-FF (100Hz, Fig. 4.8, 4.9). As already shown in Fig. 4.5 the decay was slower in young cells and gradually speeds up with postnatal development. However, the decay time constant was quite constant between different stimulation paradigms. Fig. 4.8AB and Fig. 4.9C show that the Ca^{2+} transients evoked by 1 to 10 APs decay with similar time course. With linear regression through the measured decay time constants vs AP number, the slope of the linear regression line does not significantly deviate from zero (P=0.875 for 1 week, P = 0.757 for 4 weeks).

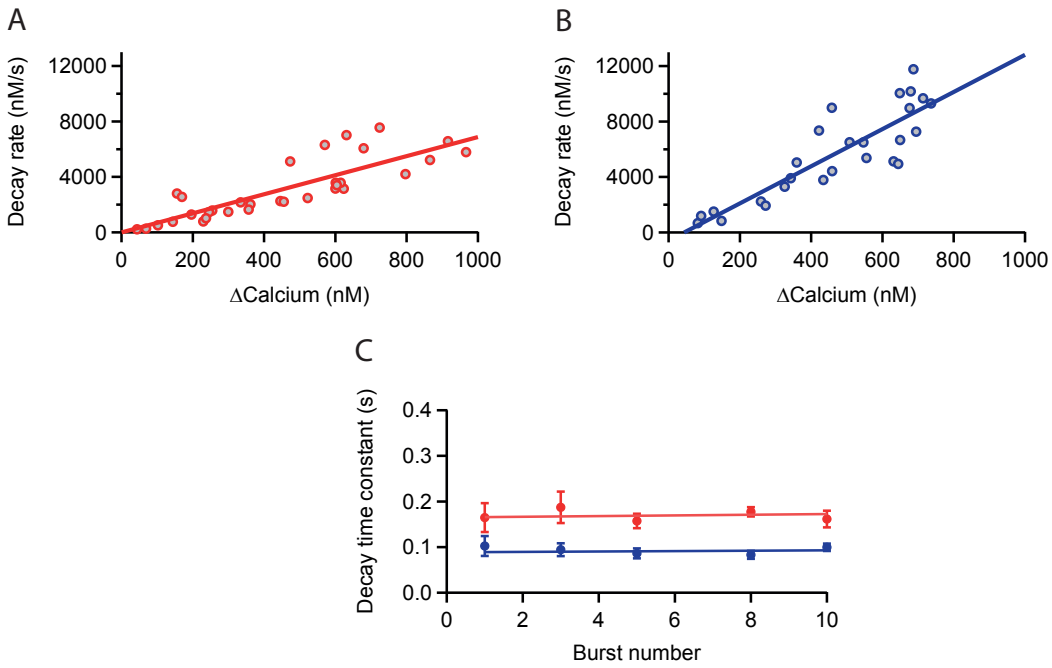

Figure 4.9: Decay time constants are independent of AP numbers in brief bursts **A**: Circles are measured decays vs relative Ca^{2+} elevation for one week old rats. Line is linear regression through the data points for different AP numbers. **B**: Circles are measured decays vs relative Ca^{2+} elevation for four weeks old rats. Line is linear regression through the data points for different AP numbers. **C**: Decay time constants after brief bursts vs number of APs in the burst. Markers are measured data ($\pm$SEM), cells from (A) and (B). Red/blue line is linear fit through the points for one/four week(s) old rats.

Thus there is no significant change of time constant with AP number (Fig. 4.9C). Next, we plotted the initial decay after the peak against the peak calcium concentration. The initial decay could be well fitted by linear regression ($r = 0.84\pm0.10$ for 1 week and $r = 0.87\pm0.10$ for 4 weeks), indicating that the Ca^{2+} extrusion rate γ is independent of Ca^{2+} concentration within the investigated range up to $\sim$1 µM. Therefore, we tried to calculate the peak amplitude of brief bursts as a linear superposition of single APs using the average amplitude of the Ca^{2+} transient evoked by a single AP measured with Fura FF and, since the decay time constant does not depend upon AP number, the average decay time constants over all AP numbers. As shown in Fig. 4.10, the simulations (red and blue line for 1 week and 4 weeks old rats) could nicely fit the measured data (grey/black), equations 3.36 and 3.37. Similarly, we calculated the total integral of dendritic Ca^{2+} signals as the linear sum of the integral of single APs which again could nicely fit the data (Fig. 4.10D). Taken together, these data suggest that during brief bursts of APs there is linear superposition of dendritic Ca^{2+} transients in developing CA1

pyramidal cells without buffer saturation or Ca^{2+} dependent modulation of Ca^{2+} influx or extrusion rate.

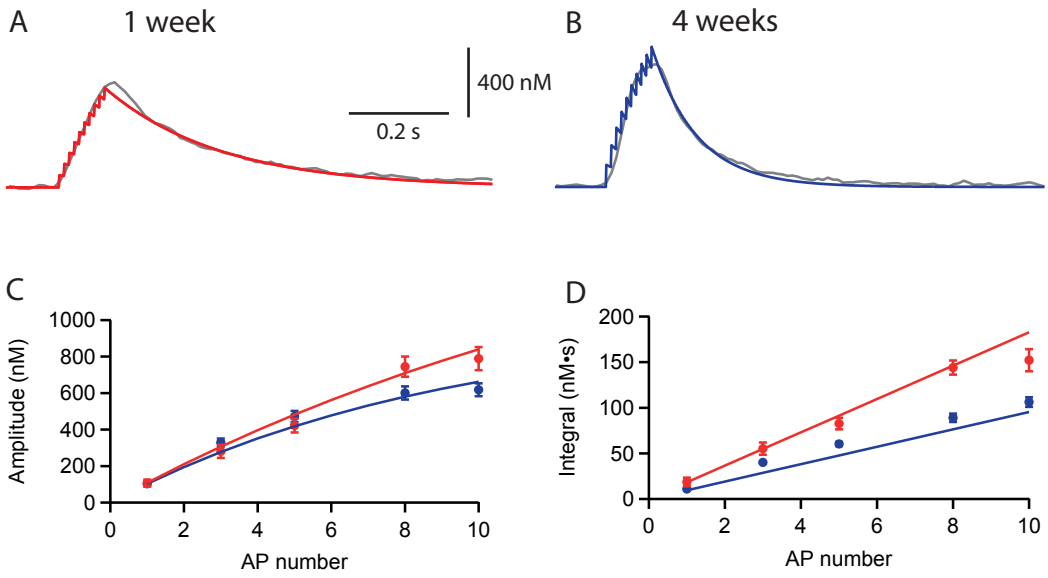

Figure 4.10: Linear summation of dendritic Ca^{2+} transients during brief bursts of APs **A**: Example trace for a one week old rat in grey. Modelled Ca^{2+} trace in red, for 10 APs at 100 Hz, using the amplitude and decay time constant for one AP from the same cell. **B**: Example of for a four weeks old rat in grey. Modelled Ca^{2+} trace in blue, for 10 APs at 100 Hz, using the amplitude and decay time constant for one AP from the same cell. **C**: Markers are measured data ($\pm$SEM, data from Fig. 4.9) for Ca^{2+} amplitude vs the burst AP number. Solid lines are the modelled values, equation 3.37. **D**: Markers are measured data ($\pm$SEM) for Ca^{2+} integral vs the burst AP number. Solid lines are the modelled values, $n \cdot A_1 \cdot \tau_1$

4.4 Activity dependent slow-down of Ca^{2+} extrusion during theta-burst firing

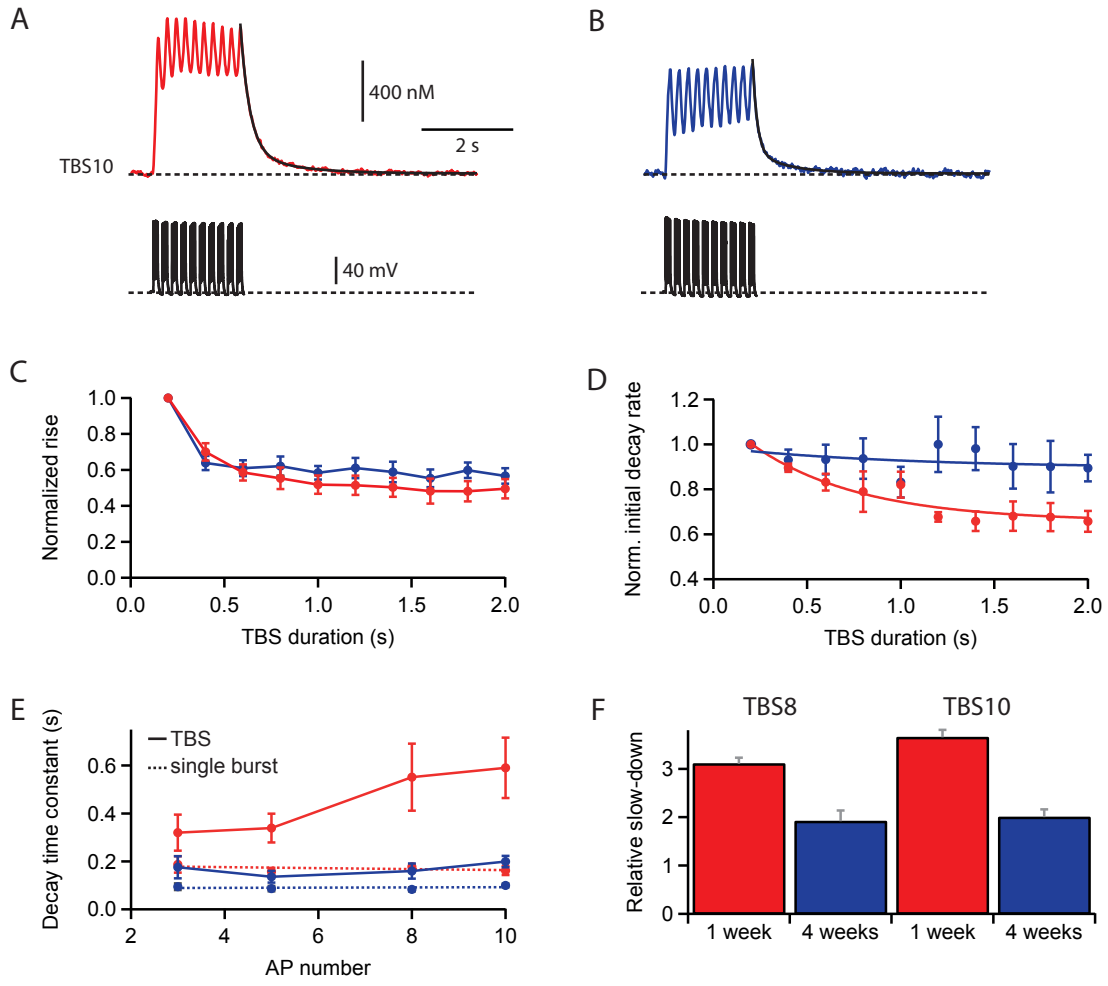

Figure 4.11: Activity dependent slow-down of extrusion during theta burst firing **A**: Example of P7 rat. *Top*: Measured Ca^{2+} transients (red) for TBS_{10}, biexponential fit (black) to the last decay. *Bottom*: Corresponding somatic membrane potential traces. **B**: As in (A) but P28 rat and measured Ca^{2+} transients in blue. **C**: Normalized rise of each TBS cycle vs bursting duration, solid lines connect measured values (±SEM). **D**: Normalized decay rate vs bursting duration. Markers (±SEM) are fit by a monoexponential function (solid lines). **E**: Markers are measured weighted decay time constants (±SEM) at the end of theta burst firing. Markers are connected by solid lines. Dashed lines are the linear regression lines through the decay time constants of brief bursts (Fig. 4.9C). **F**: Bar graphs of the ratio (±SEM) of average weighted TBS decay time constants and average brief burst decay time constant for TBS_8 and TBS_{10}.

To investigate Ca^{2+} signaling during prolonged periods of activity, we used different theta-burst stimulation paradigms (Fig. 4.11). During burst firing of APs with a repetition rate of 5 Hz we observed an initial reduction of Ca^{2+} influx for TBS_{10} after the 1st burst of APs to 70±5% and 64±4% of control in n=4 young and n=6 mature cells (Fig. 4.11C), not significantly different (P=0.35). Afterwards, however, the influx was relatively constant in 1 and in 4 weeks old rats to 50%±4 and 57%±6 at the 10th cycle, again with no significant difference between 1 and 4 weeks old rats (P=0.33).

By linearly fitting the initial decay and normalizing it to amplitude, we analyzed the initial rate of decay after each burst during TBS and found a significant reduction in initial extrusion rate to about 89±6% compared to the 1st cycle in 4 weeks old rats at the end of the TBS (Fig. 4.11D) and to 66±5% in 1 week old rats, which is significantly less (P=0.026).

In absolute numbers, the initial rate of decay reduces from the 1st to the 10th cycle from -6.3±1.1 s^{-1} to -4.0±0.5 s^{-1} in 1 week and from -9.6±1.2 s^{-1} to -8.7±1.3 s^{-1}in 4 weeks. This gradual slow-down could be fitted with a monoexponential function and developed with a time constant of T_{TBS} = 1.0 s in young and T_{TBS} = 0.58 s in mature cells.

Remarkably, fitting of the decay time course of the Ca^{2+} concentration after TBS revealed substantially larger slow-down in young cells (Fig. 4.11E, solid line, red) than in mature cells (blue). The decay after TBS showed a biexponential time course in contrast to the decay after single bursts (Fig. 4.11E, dashed lines), where the fast decay time constant of the biexponential fit reflects the initial decay rates in Fig. 4.11D. The slow decay time constant is significantly larger in young neurons (5.86±2.81 s) than in mature cells (0.59±0.08 s, P=0.0095, Mann-Whitney). The amplitude-weighted time constant after TBS_{10} was 3-times slower in young (0.59±0.13 s, n=4) than in mature cells (0.20±0.02 s , n=6, P=0.024). This slow-down of decay after TBS was more pronounced with increasing number of APs per burst, indicating that this phenomenon is Ca^{2+} dependent. The slow-down of Ca^{2+} extrusion after TBS_{10} relative to single bursts was 365±15% (n=4) in young cells and thus significantly larger than the relative slow-down in the mature cells using the same stimulation pattern (200±14% n=6, Fig. 4.11F).

In addition, we plotted Ca^{2+} extrusion rate vs the relative decrease in Ca^{2+} concentration (Fig. 4.12). Clearly, the extrusion rates are not constant.

These data show that dendritic Ca^{2+} influx and initial extrusion are slightly reduced during prolonged theta-burst activity. However, the decay-time course after TBS is substantially slower in young than in mature pyramidal cells, due to the development of a pronounced slow component in the 1-week-old neurons.

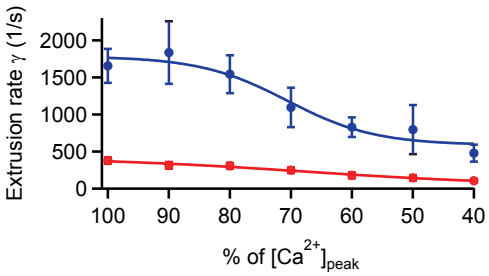

Figure 4.12: Decay phase after $[Ca^{2+}]_i$ transient induced by TBS_{10}. Red/blue markers (± SEM) are measured data from cells from Fig. 4.13. Solid lines are sigmoidal fits for young and mature cells (red and blue).

4.5 Supra-linear summation of dendritic Ca^{2+} signals in young CA1 pyramidal cells

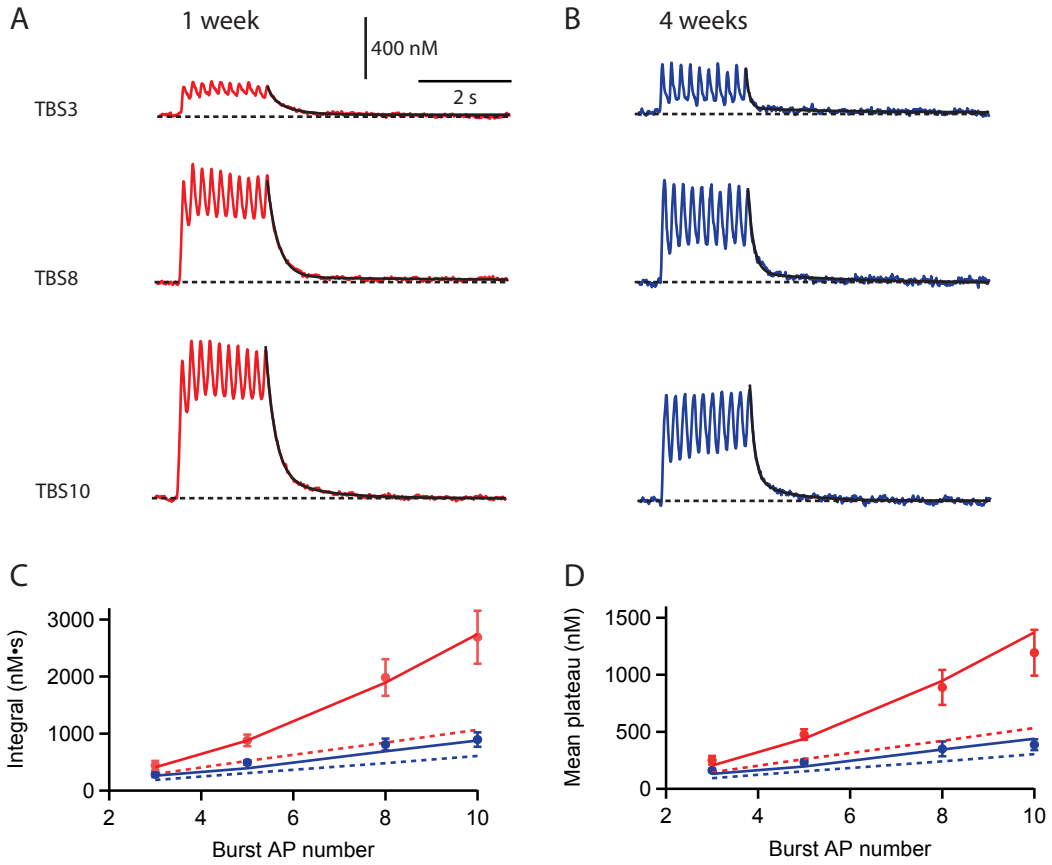

Figure 4.13: Effective temporal summation of dendritic Ca^{2+} transients in young cells. **A**: Example of P7 rat, in red measured Ca^{2+} transients for TBS_3-TBS_{10}, in black biexponential fit to the last decay. **B**: Example of P28 rat, in blue measured Ca^{2+} transients for TBS_3-TBS_{10}, in black biexponential fit to the last decay. **C**: Markers are measured data ($\pm$SEM) for Ca^{2+} integral vs burst AP number. Solid lines are the simulation with τ prolongation. Dashed lines are the simulation without τ prolongation. **D**: Markers are measured data($\pm$SEM) for Ca^{2+} mean plateau vs burst AP number for the data from (C). Solid lines are the simulation with τ prolongation. Dashed lines are the simulation without τ prolongation.

To study the consequences the activity-dependent modulation of Ca^{2+} influx and extrusion we analyzed the integral and the mean steady-state plateau levels of the dendritic Ca^{2+} signals during theta-burst stimulation (Fig. 4.13). Young cells showed substantially larger integrals (Fig. 4.13C) and mean plateau values (Fig. 4.13D) as compared to mature cells. To better understand the underlying

mechanism we tried to model Ca^{2+} accumulation based in the previously measured parameters. Without considering the activity-dependent slow-down of the Ca^{2+} extrusion during TBS (equation 3.38) the simulation revealed a linear increase of the integral and mean plateau (Fig. 4.13 CD, dashed lines). For TBS_{10} this linear prediction was similar to the measured data for mature cells (607 nM·s versus 894±126 nM·s, n=6). By contrast, in young cells the integral of TBS_{10} was 2.5-times larger than the linear prediction (1066 nM·s versus 2690±463 nM·s, n=4).

We further tried to implement the activity dependent slow-down of the decay after TBS. Therefore, we assumed that the slow time course of extrusion developed with a similar time constant T_{TBS} obtained for the slow-down of the initial decay rate (Fig. 4.11D, equation 3.39) for both ages respectively. As shown in Fig. 4.13CD the simulations (solid lines) could nicely fit the measured data. This analysis shows that the activity dependent pronounced slow-down of Ca^{2+} extrusion in young pyramidal cells is sufficient to explain the remarkable supra-linear increase of the mean plateau and total integral of the Ca^{2+} signal during theta burst firing.

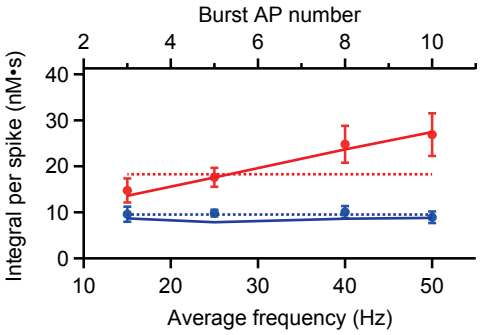

Figure 4.14: Markers (±SEM) are normalized integral per spike vs average frequency, red 1 week, blue 4 weeks old rats. Solid lines are the simulated values for the integral normalized per spike (from Fig. 4.13). Dashed lines are the integral per spike calculated from single APs measured with Fura-FF, i.e. $A_1 \cdot \tau_1$

To further visualize the supra-linearity in young cells, i.e. the deviation from 'the calcium code' (Johnston 1996), we normalized the measured Ca^{2+} integrals from Fig. 4.13 to the number of spikes during theta-burst stimulation, i.e. the integral was divided by the ten-fold burst AP number (Fig. 4.14, markers). The model from Fig. 4.13 was also normalized in such a way (Fig. 4.14, solid lines). This normalized Ca^{2+} integral per AP is plotted against the average firing frequency, i.e. the burst AP numbers times 5 Hz.

In case of four weeks old rats there is no significant change with average frequency, linear regression indicated that the slope does not significantly deviate

from zero (P=0.585). Thus, relative Ca^{2+} summation is independent of firing frequency, each AP contributes to a similar extent to the total integral of the Ca^{2+} signal and Ca^{2+} summation is linear among different TBS paradigms in four weeks old rats.

In contrast, in one week old rats linear regression reveals (P=0.009) that the slope is significantly different from zero. The normalized integral for TBS_3 against TBS_{10} and TBS_5 against TBS_{10} are significantly different (P=0.016 and P=0.002) for one week old rats. Thus, Ca^{2+} summation is non-linear among different TBS paradigms in one week old rats.

Then, we compared the normalized Ca^{2+} integral with the integral obtained by the values for a Ca^{2+} transient evoked by one AP, $A_1 \cdot \tau_1$ (Fig. 4.14, dashed lines). Again, the integral calculated with the help of A_1 and τ_1 nicely fits the measured integrals and the modelled values in four weeks old rats. This suggests that the prolongation of the decay time constant compensates for the reduction in Ca^{2+}-influx during theta burst firing in 4-week-old animals.

With one week old rats, the integral $A_1 \cdot \tau_1$ (equation 3.35) is at the level of the normalized measured integral for TBS_5, indicating that there is a small sub-linear summation with TBS_3 (due to a more pronounced reduction of normalized rise only in TBS3 in young neurons, which reduce to 0,41 at the 10^{th} cycle compared to 0.54 in four weeks old rats, P=0.02) and a huge supra-linear Ca^{2+} summation with TBS_8 and TBS_{10}.

Taken together, the results suggest that several important determinants of dendritic Ca^{2+} signalling change with postnatal development. As a consequence, 1-week-old immature pyramidal cells show substantially larger dendritic calcium signals during repetitive theta-burst firing than more mature 4-week-old neurons.

5 Discussion

5.1 Ca^{2+} handling of young neurons

We found new mechanisms how young pyramidal neurons handle Ca^{2+} to arrive from a small influx into the dendrite to huge Ca^{2+} transients. Until now, Isomura and Kato 1999; Isomura et al. 1999a; Isomura et al. 1999b only found small Ca^{2+} summation in pyramidal cells of one week old rats compared with 2-3-fold larger summation in two weeks old rats, using Fura-2, a high affinity Ca^{2+} indicator, which overwrites low endogenous buffer capacity. On the other hand, the Ca^{2+} binding ratio for the main apical dendrite of pyramidal cells in one week old rats was not known. Lee et al. 2000 found a Ca^{2+} binding ratio of 57 in a few days old cultured hippocampal neurons. In table 5.1 we compare our results with the 2 weeks old rats in Helmchen, Imoto, and Sakmann 1996. Because the calculation of κ_S from the amplitude of the Ca^{2+} transient evoked by one AP presupposes less assumptions, we include these values of κ_S in table 5.1. With respect to κ_S and $\Delta[Ca^{2+}]_T$ there is a progressive transition between one week and 3-4 weeks old rats. The A_0 is similar in one week old rats, two weeks old rats and 3-4 weeks old rats. Thus, the low Ca^{2+} influx is outbalanced by a low buffer capacity in one- to two-week-old rats. The τ_0 is already mature-like in two weeks old rats in agreement with Fig. 4.5. As seen in table 5.1 the extrusion rate γ seems to accelerate with age as well. Alternatively to the approach in Figure 4.7, γ can also be estimated from Fura-FF by equation 3.32 leading to values of 635±249 s^{-1} and 3000±597 s^{-1} for 1- and 4-week-old rats, respectively (table 5.1). The values for γ calculated

age of rats	1 week	2 weeks	3-4 weeks
κ_S (from A^{-1})	69 (± 52)	168 (± 61)	276 (± 45)
$[Ca^{2+}]_T$ [µM]	10 (± 2)	26 (± 10)	44 (± 5)
A_0 [nM]	137 (± 101)	151 (± 19)	160 (± 18)
τ_0 [ms]	170 (± 9)	92 (± 25)	93 (± 5)
γ [1/s]	635 (± 249)	1837 (± 830)	3000 (± 597)

Table 5.1: Comparison of buffer capacities with literature. In the left and right column results from Fig. 4.7 are plotted against Helmchen, Imoto, and Sakmann 1996 in the middle column. For τ_0 and γ we plotted the values obtained from Fura-FF measurements.

from our buffer capacity experiments (Fig. 4.7) mainly done with Fura-2 are only about half of the extrusion rates indicated in table 5.1.

How can this difference in extrusion rates be accounted for? Fura-2 is a high affinity Ca^{2+} indicator. The different K_d of Fura-2 and Fura-FF is caused by a k_{off}-rate which is 14-times slower for Fura-2. Thus, Fura-2 has a k_{off}-rate of only $\sim$100 per second. A typical value of Ca^{2+} resting concentration is 50 nM, a typical value for the relative Ca^{2+} amplitude using 100 µM Fura 2 is 100 nM, giving rise to $[Ca^{2+}]_i$=150 nM. Fura-2 has a K_d of 286 nM. From equation 3.16 and 3.14 it is evident that at peak Ca^{2+} concentration typically one third of the Ca^{2+} ions are bound to Fura-2. At peak Ca^{2+} concentrations the apparent Ca^{2+} extrusion rate is thus diminished by Fura-2.

If this is only a problem for our measured 3-4 weeks old rats or already for the two weeks old rats in Helmchen, Imoto, and Sakmann 1996 remains unclear. The mature-like τ_0 in two weeks old rats indicates that the extrusion rate γ is underestimated in the two weeks old rats as well by the usage of Fura-2.

κ_S in the main apical dendrite increases with age, but the Ca^{2+} binding ratio in spines seems to stay at a low value of $\sim$20 with growing age (Cornelisse et al. 2007 for P6-P15 and Sabatini, Oertner, and Svoboda 2002 for P14-P20). This may suggest that Ca^{2+} dependent plastic processes decrease during postnatal development in the mean apical dendrite, while the spines stay plastic. To my knowledge, there are no measurements of the Ca^{2+} binding ratio in spines in older animals.

Our results in young neurons are different from young dentate gyrus granule cells which exhibit a speed-up of decay time constant with increasing AP number (Stocca, Schmidt-Hieber, and Bischofberger 2008).

In CA1 pyramidal cells, backpropagation of APs decreases with activity (Golding et al. 1999; Golding and Spruston 1998 and combined with dendritic Ca^{2+} imaging in Spruston et al. 1995) due to a slow recovery from inactivation of dendritic voltage-gated sodium channels and the high dendritic expression density of A-type potassium channels. The linear superposition of Ca^{2+} (Fig. 4.10) suggests that we do not have any failure or severe reduction of action potential backpropagation at 100 µm during a burst of APs which is remarkable in the young neurons since they probably express less voltage gated sodium channels.

5.2 Non-linear Ca^{2+} summation

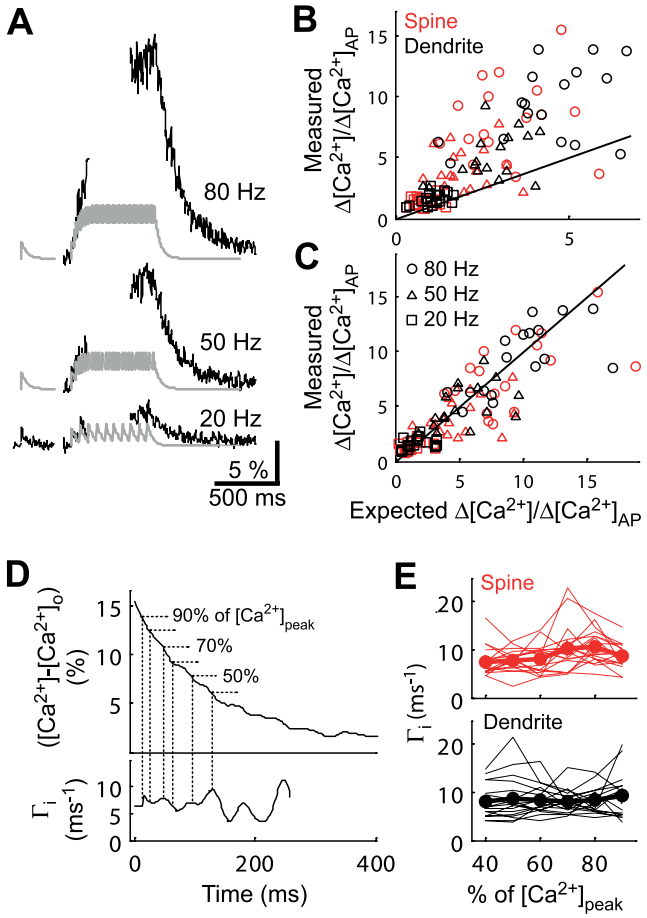

Figure 5.1: Activity-dependent slowing of the decay of Ca^{2+} transients. **A** Comparison of measured $[Ca^{2+}]_i$ transients (black) and simulated $[Ca^{2+}]_i$ transients (grey). Simulations were based on the amplitude and decay time of the Ca^{2+} transient evoked by a single AP. **B** Measured mean plateau levels vs simulated mean plateau levels, based on the amplitude and decay time of the Ca^{2+} transient evoked by a single AP. The black line shows equality. The measured mean plateau levels are larger than the simulated. **C** Same as (B), except the calculation used the decay time of the Ca^{2+} transient at the end of AP trains. The black line shows equality. Measured and simulated mean plateau levels are concordant. **D** *Top*: The decay phase of a Ca^{2+} transient evoked by an 80 Hz AP train in a spine (baseline subtracted). *Bottom*: Corresponding extrusion rate γ vs time. Dotted lines indicate amplitude levels as a percentage of peak Ca^{2+}. **E** γ vs $\Delta[Ca^{2+}]_i$ level (percentage of peak $[Ca^{2+}]_i$). Figure and legend modified from Scheuss et al. 2006.

Scheuss et al. 2006 found non-linear $[Ca^{2+}]_i$ summation in small dendrites and spines of P16-P20 rats. They also found an activity-dependent slow-down of Ca^{2+} extrusion, in small dendrites and spines, during AP firing at different frequencies for around 800 ms (Fig. 5.1). We found on the one hand after single brief 100 Hz bursts (up to 100 ms) no substantial activity-dependent slow-down. This leads us to conclude, that 100 ms stimulation duration is too short to induce decay time prolongation, indicating that decay time prolongation is not purely dependent on Ca^{2+} concentration but on duration of stimulation.

For our theta-burst stimulation we calculated the average frequency (Fig. 4.14) which is in a comparable range with Scheuss et al. 2006. We also came to the conclusions as in Fig. 5.1A-C. In contrast to them, we do not think that this activity-dependent slow-down is a general mechanism but is restricted to early postnatal development (first three weeks) as seen in Fig. 4.14. For our 4 weeks old rats in Fig. 4.14 we do not observe a mismatch between Ca^{2+} integrals expected from single APs and measured Ca^{2+} integrals as they see in Fig. 5.1BC for P16-P20 rats. Their is still some slow-down of the decay-time constant during theta-burst stimulation in 4 weeks old rats, but this is perfectly compensated by the reduction in Ca^{2+} influx. In contrast, Fig. 4.14 clearly shows the non-linear Ca^{2+} signaling in our one week old rats in agreement with 5.1BC.

Scheuss et al. 2006 discussed that Helmchen, Imoto, and Sakmann 1996 and Maravall et al. 2000 overlooked the effect of non-linear Ca^{2+} summation due to technical reasons (see section 5.4). Since Helmchen, Imoto, and Sakmann 1996 and Maravall et al. 2000 measured Ca^{2+} transients in the main apical dendrite, Scheuss et al. 2006 is likely to believe that they found a general principle also relevant for the main apical dendrite. This would be contradicting our findings in four weeks old rats (Fig. 4.14), restricting Scheuss et al. 2006 findings to the first 3 weeks of postnatal development.

However, there is a second possibility. Scheuss et al. 2006 and our findings of non-linear Ca^{2+} summation might be restricted to relatively small dendrites and spines. In this view, we would not see any supra-linear Ca^{2+} summation in four weeks old rats (Fig. 4.14) because diameter of the main apical dendrite has become too large. From our measurements, we are not able to discriminate between the two possible explanations.

In addition, Scheuss et al. 2006 made the assumption that $\Delta[Ca^{2+}]_{AP}$, the amplitude of the Ca^{2+} transient evoked by a single AP, remained constant during their bursts. They claimed that

> "this assumption is supported by the observation that the measured $[Ca^{2+}]$ plateau levels and those predicted based on unchanged $\Delta[Ca^{2+}]_{AP}$ match"

(Scheuss et al. 2006). Comparing our Fig. 4.11C and Fig. 4.14, the four weeks

old rats seem to perfectly match the expected integrals and therefore also the mean plateau levels when comparing measured and simulated values, with the latter taken the amplitude and the decay time constant of single APs (figure 4.14). On the other hand, Ca^{2+} amplitudes reduce from theta-burst cycle to theta-burst cycle (Fig. 4.11C). This is perfectly matched by a prolongation of the amplitude-weighted decay time constants (4.11D). Because Scheuss et al. 2006 can simulate the correct mean plateau level only by prolonging the decay time constant (5.1) without considering a reduction of $\Delta[Ca^{2+}]_{AP}$, there are two possibilities: Either Scheuss et al. 2006 overlooked the effect of amplitude reduction because it is covered by the decay time prolongation. Or second, there are different mechanisms responsible in the main apical dendrites versus thin dendrites and spines.

Scheuss et al. 2006 evaluated the mean plateau level from Ca^{2+} traces that lasted ~800 ms. In Fig. 5.1A (black traces) the mean plateau level does not look like a steady-state level already reached and thus their approach of simulation may be inexact. Therefore, I think that they overlooked the effect of amplitude reduction during prolonged activity.

The successful simulation of Ca^{2+} integration (Fig. 4.8 and 4.13) suggests that Ca^{2+} dependent Ca^{2+} release does not substantially contribute to our Ca^{2+} summation in agreement with Sabatini and Svoboda 2000 and in contrast to Sandler and Barbara 1999.

5.3 Ca^{2+} buffer capacity in interneurons and principal neurons

There are several groups claiming a difference in Ca^{2+} buffer capacity between interneurons and principal cells. Lee et al. 2000 claimed such a difference for interneurons ($\kappa_S \approx 130$) vs principal neurons ($\kappa_S \approx 57$) in a few days old hippocampal culture, Kaiser, Zilberter, and Sakmann 2001 for bitufted interneurons ($\kappa_S \approx 285$) vs layer 2/3 pyramidal cells ($\kappa_S \approx 185$) (P14-P16), Rozsa et al. 2004 for CA1 pyramidal neurons ($\kappa_S \approx 27$) vs CA stratum radiatum interneurons ($\kappa_S \approx 71$) (P16-P19) and Aponte, Bischofberger, and Jonas 2008 stated a Ca^{2+} buffer capacity of 202 in fast-spiking, parvalbumin positive basket cells (P18-P21).

Principal neurons on the other hand are reported to exhibit lower buffer capacity, as for layer V pyramidal cells ($\kappa_S \approx 116$) and CA1 pyramidal cells ($\kappa_S \approx 178$) (in Helmchen, Imoto, and Sakmann 1996, P12-P14), in apical dendrites of CA1 pyramidal neurons $\kappa_S \approx 61$ (Maravall et al. 2000, P14-P28) and $\kappa_S \approx 112$ in basal dendrites of layer 2/3 pyramidal cells (P13-P15).

Furthermore, inhibitory neurons are reported to be less plastic and more stable than excitatory cells (McBain, Freund, and Mody 1999).

Our measurements indicate (table 5.1) that the proposed difference in Ca^{2+}

buffer capacity between excitatory and inhibitory neurons is not a general principle but a matter of postnatal development with the inhibitory neurons more rapidly up-regulating Ca^{2+} binding ratios and the excitatory neurons gain buffer capacity to the same values of more than 200 as interneurons (table 5.1) but several days later.

Does this also mean that the plastic properties of mature-like pyramidal cells reduce as well with increasing κ_S? On the one hand dendrites in older mice (P42-P51) are very stable when observed over four weeks (Wilbrecht et al. 2010). This is in favour of our view that with growing Ca^{2+} buffer capacity dendritic plasticity is reduced. On the other hand it is reported that in spines and in very small dendrites the buffer capacity is lower than in the main apical dendrite (Sabatini, Oertner, and Svoboda 2002), being 20, 60 and 180 in spines, small dendrites and the main apical dendrite in 2-3 weeks old rats. Thus at least spines might stay with a low buffer capacity when the animal gets older, which is consistent with spine plasticity in Wilbrecht et al. 2010.

In addition, there is a contradiction between the Ca^{2+} buffer capacity of 238 in our measurements for 4 weeks old rats (table 4.1) and a Ca^{2+} buffer capacity of 44 as well for apical dendrites for CA1 pyramidal cells in P24-P28 rats (Maravall et al. 2000). They did not use ratiometric Fura-imaging to observe Ca^{2+} buffer capacity but OGB-1 which is a Ca^{2+} indicator without Ca^{2+}-independent isosbestic wave length. In order to calibrate OGB-1 they used AP trains to saturate the Ca^{2+} indicator and assumed constant Ca^{2+} amplitudes within the AP train. As we showed in Fig. 4.11C Ca^{2+} amplitudes diminish during AP trains. Thus, the OGB-1 method for determining the Ca^{2+} buffer capacity might be inexact which is also reflected in Fig. 6B of Maravall et al. 2000. In older animals (P24-P28) they got a convex curve instead of a line when plotting the inverse Ca^{2+} amplitude against κ_B (equation 3.33).

Aponte, Bischofberger, and Jonas 2008 reported a total calcium load $\Delta[Ca^{2+}]_T$ of only 8 µM in fast-spiking, parvalbumin-positive basket cells, on the other hand we found in 3-4 weeks old rats which also have a high buffer capacity as the basket cells an age-dependent increase in the total calcium load to 44 µM. The higher total calcium load in pyramidal neurons of 3-4 weeks old rats together with their high Ca^{2+} buffer capacity reduces Ca^{2+} summation during brief bursts, but suggests that Ca^{2+} summation during prolonged activity is still huge enough to induce plasticity (Fig. 4.13), especially since the mean plateau level of Ca^{2+} summation during bursts for several seconds is usually independent of Ca^{2+} buffer capacity, but dependent on influx and extrusion (Tank, Regehr, and Delaney 1995; Helmchen, Imoto, and Sakmann 1996; Helmchen and Konnerth 2011).

Also, it should be stated that interneurons bear great diversity. Regular-spiking, CCK-positive basket cells in the CA1 region of P15-P30 mice only have a Ca^{2+}

buffer capacity of 74 and Schaffer-collateral associated interneurons showed a buffer capacity of 179 (Evstratova, Chamberland, and Topolnik 2011), which is very similar to CA1 pyramidal cells of P12-P14 (Helmchen, Imoto, and Sakmann 1996) and less than we found in 3-4 weeks old CA1 pyramidal cells (table 4.1). Furthermore, for oriens-lacunosum moleculare-interneurons in P16-P21 rats Liao and Lien 2009 only measured a Ca^{2+} buffer capacity of ∼22, enabling these O-LM-interneurons to generate large Ca^{2+} transients having only a total calcium load of 12 µM, but this makes O-LM-interneurons susceptible for damage in epileptic seizures (Gee, Woodhall, and Lacaille 2001; Woodhall et al. 1999). On the other hand, basket cells with their high Ca^{2+} buffer capacity are more robust against epileptic seizures and even get hyperactive, whereas O-LM interneurons with their low buffer capacity are partially lost after epileptic seizures (Cossart et al. 2001). Thus, the high Ca^{2+} buffer capacity in 3-4 week old rats may also protect the CA1 pyramidal cells from seizures as the network matures and more connections are acquired.

In summary, there exist also groups of interneurons with a Ca^{2+} buffer capacity lower than in principal neurons, and excitatory neurons seem to gain the same high Ca^{2+} buffer capacity as fast-spiking basket cells, for example.

5.4 Possible mechanisms of slow-down of Ca^{2+} extrusion

In dendrites of CA1 pyramidal neurons Na^+/Ca^{2+} exchangers (NCX, NCKX) and plasma-membrane-Ca^{2+}-ATPases (PMCAs) are the most important extrusion mechanisms for Ca^{2+} (Scheuss et al. 2006).

The Na^+/Ca^{2+} exchanger has a relative low affinity for transport of up to 1.4 mM (Blaustein and Lederer 1999). There are two diverse groups of Na^+/Ca^{2+} exchangers. NCX exchangers with a stoichiometric ratio of 3:1 and NCKX with a stoichiometric ratio of 4:1:1 (Blaustein and Lederer 1999; Lytton et al. 2002; Scheuss et al. 2006). It is known that at least NCX2 (Jeon et al. 2003) and NCX3 (Canitano et al. 2002; Papa et al. 2003; Scheuss et al. 2006) exist on dendrites of CA1 pyramidal neurons.

Without calmodulin bound to Ca^{2+}, PMCAs also have a low affinity for Ca^{2+} with a K_d of about 10 µM (Carafoli 1992). Calmodulin is the fastest Ca^{2+} sensor in the cell (Faas et al. 2011) and due to a calmodulin concentration of about 10-100 µM (Xia and Storm 2005, Scheuss et al. 2006), most of the PMCAs will change their K_d values to ∼0.1 to 1.0 µM (Carafoli 1992; Caride et al. 2001, Scheuss et al. 2006) switching to a high affinity for Ca^{2+}-calmodulin and thus the PMCAs will mostly be saturated at the peak Ca^{2+} concentrations in Fig. 4.13.

Then, PMCAs have a more than 10 times lower transport rate than Na^+/Ca^{2+} exchangers, but a 10-fold higher affinity (Blaustein and Lederer 1999; Scheuss et al. 2006). Therefore one usually assumes that the Na^+/Ca^{2+} exchangers are responsible for the first fast component of Ca^{2+} extrusion and the PMCAs are responsible for slower Ca^{2+} extrusion during a later phase of clearance (Thayer, Usachev, and Pottorf 2002). In contrast, Scheuss et al. 2006 found that Na^+/Ca^{2+} exchangers and PMCAs equally contribute to Ca^{2+} extrusion which is consistent with Fig. 5.1DE where Scheuss et al. 2006 did not find any change in Ca^{2+} extrusion rate during the decay of the Ca^{2+} transients from 90% to 40% of peak Ca^{2+} level. On the contrary we found at least two distinct Ca^{2+} extrusion rates after the theta-burst stimulation (Fig. 4.12), fast extrusion at high Ca^{2+} levels (∼ 90% of maximal Ca^{2+} level) and slow Ca^{2+} extrusion at around 50% of the Ca^{2+} level, being consistent with the classical view of Thayer, Usachev, and Pottorf 2002. This difference between our data and Scheuss et al. 2006 data might emerge from the examined structures. Scheuss et al. 2006 examined small dendrites and spines, we examined the larger main apical dendrite, which has a larger volume perhaps avoiding a high accumulation of sodium as with Scheuss et al. 2006, thus leaving the Na^+/Ca^{2+} transport rate intact and not mixing impaired Na^+/Ca^{2+} exchanger activity with PMCAs contribution, which might have led to the apparant constant extrusion rate in Fig. 5.1DE.

Helmchen, Imoto, and Sakmann 1996 observed only a small prolongation of decay time constant after AP bursts which lasted for 2 s, the same duration we took for theta-burst stimulation (Fig. 4.11 and Fig. 4.13). They compared the expected mean plateau (using the amplitude and the decay time constants from a single action potential) with the measured mean plateau during the AP bursts. A similar comparison (Fig. 4.14) revealed to us a perfect equality between the expected integral (using the amplitude and the decay time constants from single action potentials) with the measured integrals, only for 4 weeks old animals. Thus, it might be that already at P12-P14 the summation is linear as in our 4 weeks old rats which would be a contradiction to Scheuss et al. 2006. Scheuss et al. 2006 dissolved this contradiction with the different use of Ca^{2+} indicators. Helmchen, Imoto, and Sakmann 1996 used the high affinity Ca^{2+} indicator Fura-2 which disturbs the endogenous Ca^{2+} buffer capacity and thus could have prevented the effect of non-linear summation.

In addition, Helmchen, Imoto, and Sakmann 1996 only used 100 µM of Fura-2 and measured Ca^{2+} concentration of $\sim$ 500 nM which might lead to buffer saturation which would speed up decay time constants and thus reducing a prolongation of decay time constants with activity. Furthermore, it might not be appropriate to compare the main apical dendrite in Helmchen, Imoto, and Sakmann 1996 with the thin dendrites and spines in Scheuss et al. 2006.

The same argumentation holds true for Maravall et al. 2000. They used the high-affinity Ca^{2+} indicator OGB-1 and found no sign of prolongation of decay time constants after bursts of APs.

5.5 Functional role of activity-dependent slow-down

Our findings of enhanced Ca^{2+} summation in young neurons are important for three aspects. First, Ca^{2+} triggers dendritic development. Comparing the anatomy of pyramidal cells from one week old rats and two weeks and older rats (Fig. 2.6), there is a huge buildup of new dendritic branches from the apical dendrite. Ca^{2+} is a very important messenger molecule to trigger dendritic development (Fig. 2.7). At the age of one week the input to the rats from their surroundings is still reduced. Thus, the young neurons can very effectively sum up already mild physiological signals. Glutamate-induced spinogenesis is facilitated via Ras activated by Ca^{2+} influx in young neurons (P7-P12), extenuated at P14-P15 and unsuccessful at P19-P20 in neocortical pyramidal neurons (Kwon and Sabatini 2011), consistent with morphological studies (Miller 1981). In addition, the dendritic structure in mature rats is much more conserved and only the spines stay as plastic elements (Wilbrecht et al. 2010).

Second, LTP can be induced in young granule cells with milder theta-burst-pairing than in mature granule cells which require more spiking (Schmidt-Hieber, Jonas, and Bischofberger 2004).

In mammalian excitatory neurons there is an interchange of Ca^{2+} from the dendrite to the spines (Bloodgood and Sabatini 2005) making it possible that dendritic Ca^{2+} integration might boost synaptic plasticity. Small postsynaptic Ca^{2+} elevations tend to induce LTD, large postsynaptic Ca^{2+} elevations tend to induce LTP (Johnston et al. 2003; Cummings et al. 1996). Dendritic Ca^{2+} spikes are important for the induction of spike-timing-dependent plasticity (Kampa, Letzkus, and Stuart 2006). Even in the first postnatal week, nascent glutamatergic synapses express both functional AMPA and NMDA receptors (Groc, Gustafsson, and Hanse 2002).

Currently, experiments of long-term plasticity in 1 week old rats are limited. In P6-P12 rats it is substantially easier to induce LTD with low-frequency stimulation than in P27-P42 (Wasling, Hanse, and Gustafsson 2002). Both negative as well as positive delays between AP-EPSP led to LTP in somatosensory pyramidal cells of rats aged P7-P12, however, with P15-P21 there was a switch to LTP with positive AP-EPSP delay and LTD with negative AP-EPSP delay (Itami and Kimura 2012). This supports our view of the one week old rats exhibiting enlarged plasticity and learning and older rats being able to more subtle discriminate stimuli via sharper Ca^{2+} transients.

Even at the age of two weeks (P14-P16), the very mild pairing patterns from Bi and Poo 1998 used in acute slices for CA1 pyramidal cells still induced LTP (Fuenzalida et al. 2010). But Fuenzalida et al. 2010 needed to depolarize the holding potential to -65 mV and repeat the induction paradigm for one minute as a sign that LTP induction with only one EPSP paired with one AP is quite a weak paradigm. Raising the number of APs, two-week-old rats still show a supralinear Ca^{2+} summation as our one-week-old rats (Scheuss et al. 2006; own data not shown in this manuscript). However, Wittenberg and Wang 2006 showed with CA1 pyramidal cells in P14-P21 rats, being only a few days older on average than in Fuenzalida et al. 2010, that pairing single presynaptic and postsynaptic action potential only induces LTD and that one needed stronger pairing at theta-burst frequency. This is consistent with our view that 3-4 weeks old rats have a high Ca^{2+} buffer capacity requiring stronger induction paradigms.

Raymond 2007 claimed that long-lasting LTP in CA1 pyramidal cells would require dendritic participation which is consistent with our view of relieved LTP induction in young animals and enhanced threshold for LTP induction mechanisms in older rats, helping the young animals for expeditious learning.

Third, regarding the sensitivity of one week old rats to damages due to too much activity (Seifert et al. 2009, Sipilä et al. 2009) the young neurons manage to generate the huge Ca^{2+} transients which are necessary for dendritic development in an energy-efficient way. Low total calcium load per AP together with small buffer capacity generates large calcium signals which can be cleared with relatively small ATP-consumption. Furthermore, activity-dependent decrease of Ca^{2+}-influx and slow-down of extrusion during prolonged activity further generates energy-efficient calcium signalling during repetitive AP firing. This is also important for the CA3 neurons which are sending their axons as Schaffer-collaterals to the CA1 pyramidal cells and thus stimulating them. But presynaptic processes, i.e., Ca^{2+} clearance, transmitter uptake and vesicle recycling have a similar proportion on energy consumption at synaptic transmission as presynaptic APs at the CA3-CA1 synapses (Liotta et al. 2012). In summary, young neurons might overcome energy limitations by our finding of activity dependent decrease of Ca^{2+}-influx and slow-down of Ca^{2+}-extrusion, finally leading to energy-efficient calcium dependent plasticity processes.

Bibliography

Amaral, D. G. (1999). "Introduction: what is where in the medial temporal lobe?" *Hippocampus* 9.1, pp. 1–6.

Andersen, Per et al., eds. (2006). *The hippocampus book*. Oxford University Press.

Aponte, Yexica, Bischofberger, Josef, and Jonas, Peter (2008). "Efficient Ca^{2+} buffering in fast-spiking basket cells of rat hippocampus." *J Physiol* 586.8, pp. 2061–2075.

Bartos, Marlene et al. (2002). "Fast synaptic inhibition promotes synchronized gamma oscillations in hippocampal interneuron networks." *Proc Natl Acad Sci U S A* 99.20, pp. 13222–13227.

Bi, G. Q. and Poo, M. M. (1998). "Synaptic modifications in cultured hippocampal neurons: dependence on spike timing, synaptic strength, and postsynaptic cell type." *J Neurosci* 18.24, pp. 10464–10472.

Bischofberger, Josef et al. (2006). "Patch-clamp recording from mossy fiber terminals in hippocampal slices." *Nat Protoc* 1.4, pp. 2075–2081.

Blaustein, M. P. and Lederer, W. J. (1999). "Sodium/calcium exchange: its physiological implications." *Physiol Rev* 79.3, pp. 763–854.

Bloodgood, Brenda L. and Sabatini, Bernardo L. (2005). "Neuronal activity regulates diffusion across the neck of dendritic spines." *Science* 310.5749, pp. 866–869.

Briz, Victor et al. (2013). "Calpain-2-Mediated PTEN Degradation Contributes to BDNF-Induced Stimulation of Dendritic Protein Synthesis." *J Neurosci* 33.10, pp. 4317–4328.

Brockmann, Marco D. et al. (2011). "Coupled oscillations mediate directed interactions between prefrontal cortex and hippocampus of the neonatal rat." *Neuron* 71.2, pp. 332–347.

Canitano, Adriano et al. (2002). "Brain distribution of the Na^{+}/Ca^{2+} exchanger-encoding genes NCX1, NCX2, and NCX3 and their related proteins in the central nervous system." *Ann N Y Acad Sci* 976, pp. 394–404.

Carafoli, E. (1992). "The Ca^{2+} pump of the plasma membrane." *J Biol Chem* 267.4, pp. 2115–2118.

Caride, A. J. et al. (2001). "Delayed activation of the plasma membrane calcium pump by a sudden increase in Ca^{2+}: fast pumps reside in fast cells." *Cell Calcium* 30.1, pp. 49–57.

Casale, Amanda E. and McCormick, David A. (2011). "Active action potential propagation but not initiation in thalamic interneuron dendrites." *J Neurosci* 31.50, pp. 18289–18302.

Chiovini, Balázs et al. (2010). "Enhanced dendritic action potential backpropagation in parvalbumin-positive basket cells during sharp wave activity." *Neurochem Res* 35.12, pp. 2086–2095.

Cornelisse, L Niels et al. (2007). "High speed two-photon imaging of calcium dynamics in dendritic spines: consequences for spine calcium kinetics and buffer capacity." *PLoS One* 2.10, p. 1073.

Cossart, R. et al. (2001). "Dendritic but not somatic GABAergic inhibition is decreased in experimental epilepsy." *Nat Neurosci* 4.1, pp. 52–62.

Cummings, J. A. et al. (1996). "Ca^{2+} signaling requirements for long-term depression in the hippocampus." *Neuron* 16.4, pp. 825–833.

Evstratova, Alesya, Chamberland, Simon, and Topolnik, Lisa (2011). "Cell type-specific and activity-dependent dynamics of action potential-evoked Ca^{2+} signals in dendrites of hippocampal inhibitory interneurons." *J Physiol* 589.Pt 8, pp. 1957–1977.

Faas, Guido C. et al. (2011). "Calmodulin as a direct detector of Ca^{2+} signals." *Nat Neurosci* 14.3, pp. 301–304.

Feldman, Daniel E. (2012). "The spike-timing dependence of plasticity." *Neuron* 75.4, pp. 556–571.

Fuenzalida, Marco et al. (2010). "Reply to Meredith and Groen: Role of AMPA and NMDA Receptors and Back-Propagating Action Potentials in Spike Timing-Dependent Plasticity." *J Neurophysiol* 103.4, p. 2314.

Ge, Shaoyu et al. (2007). "A critical period for enhanced synaptic plasticity in newly generated neurons of the adult brain." *Neuron* 54.4, pp. 559–566.

Gee, C. E., Woodhall, G., and Lacaille, J. C. (2001). "Synaptically activated calcium responses in dendrites of hippocampal oriens-alveus interneurons." *J Neurophysiol* 85.4, pp. 1603–1613.

Ghosh, A. and Greenberg, ME (1995). "Calcium signaling in neurons: molecular mechanisms and cellular consequences". *Science*, pp. 239–47.

Golding, N. L. and Spruston, N. (1998). "Dendritic sodium spikes are variable triggers of axonal action potentials in hippocampal CA1 pyramidal neurons." *Neuron* 21.5, pp. 1189–1200.

Golding, N. L. et al. (1999). "Dendritic calcium spike initiation and repolarization are controlled by distinct potassium channel subtypes in CA1 pyramidal neurons." *J Neurosci* 19.20, pp. 8789–8798.

Groc, Laurent, Gustafsson, Bengt, and Hanse, Eric (2002). "Spontaneous unitary synaptic activity in CA1 pyramidal neurons during early postnatal develop-

ment: constant contribution of AMPA and NMDA receptors." *J Neurosci* 22.13, pp. 5552–5562.

Grynkiewicz, G., Poenie, M., and Tsien, R. Y. (1985). "A new generation of Ca2+ indicators with greatly improved fluorescence properties." *J Biol Chem* 260.6, pp. 3440–3450.

Gustafson, G.B. and Wilcox, C.H. (1998). *Analytical and Computational Methods of Advanced Engineering Mathematics*.

Hammond, Constance, ed. (2008). *Cellular and Molecular Neurophysiology*. Academic Press.

Helmchen, F., Imoto, K., and Sakmann, B. (1996). "Ca^{2+} buffering and action potential-evoked Ca^{2+} signaling in dendrites of pyramidal neurons." *Biophys J* 70.2, pp. 1069–1081.

Helmchen, F. and Konnerth, A. (2011). *Imaging in Neuroscience. A laboratory manual. Chapter 36: A single-compartment model of calcium dynamics in nerve terminals and dendrites*. Ed. by R. Yuste. Cold spring harbor laboratory press, pp. 355–368.

Hensch, Takao K. (2005a). "Critical period mechanisms in developing visual cortex." *Curr Top Dev Biol* 69, pp. 215–237.

– (2005b). "Critical period plasticity in local cortical circuits." *Nat Rev Neurosci* 6.11, pp. 877–888.

Higley, Michael J. and Sabatini, Bernardo L. (2012). "Calcium signaling in dendritic spines." *Cold Spring Harb Perspect Biol* 4.4, a005686.

Häusser, M. et al. (1995). "Axonal initiation and active dendritic propagation of action potentials in substantia nigra neurons." *Neuron* 15.3, pp. 637–647.

Huxter, John, Burgess, Neil, and O'Keefe, John (2003). "Independent rate and temporal coding in hippocampal pyramidal cells." *Nature* 425.6960, pp. 828–832.

Isomura, Y. and Kato, N. (1999). "Action potential-induced dendritic calcium dynamics correlated with synaptic plasticity in developing hippocampal pyramidal cells." *J Neurophysiol* 82.4, pp. 1993–1999.

Isomura, Y. et al. (1999a). "Developmental regulation of action potential-induced Ca^{2+} entry in neocortical neurons." *Neuroreport* 10.9, pp. 1947–1950.

Isomura, Y. et al. (1999b). "Postnatal development of action potential-induced dendritic calcium entry in neocortical layer II/III pyramidal cells." *Brain Res* 832.1-2, pp. 175–178.

Itami, Chiaki and Kimura, Fumitaka (2012). "Developmental switch in spike timing-dependent plasticity at layers 4-2/3 in the rodent barrel cortex." *J Neurosci* 32.43, pp. 15000–15011.

Jensen, Thomas P, Buckby, Lucy E, and Empson, Ruth M (2004). "Expression of plasma membrane Ca^{2+} ATPase family members and associated synaptic

proteins in acute and cultured organotypic hippocampal slices from rat." *Brain Res Dev Brain Res* 152.2, pp. 129–136.

Jeon, Daejong et al. (2003). "Enhanced learning and memory in mice lacking Na^+/Ca^{2+} exchanger 2." *Neuron* 38.6, pp. 965–976.

Jezek, Karel et al. (2011). "Theta-paced flickering between place-cell maps in the hippocampus." *Nature* 478.7368, pp. 246–249.

Jin, Ming et al. (2005). "Ca^{2+}-dependent regulation of rho GTPases triggers turning of nerve growth cones." *J Neurosci* 25.9, pp. 2338–2347.

Johnston, D. (1996). "The calcium code." *Biophys J* 70.3, p. 1095.

Johnston, Daniel et al. (2003). "Active dendrites, potassium channels and synaptic plasticity." *Philos Trans R Soc Lond B Biol Sci* 358.1432, pp. 667–674.

Kaiser, K. M., Zilberter, Y., and Sakmann, B. (2001). "Back-propagating action potentials mediate calcium signalling in dendrites of bitufted interneurons in layer 2/3 of rat somatosensory cortex." *J Physiol* 535, pp. 17–31.

Kampa, Björn M, Letzkus, Johannes J, and Stuart, Greg J (2006). "Requirement of dendritic calcium spikes for induction of spike-timing-dependent synaptic plasticity." *J Physiol* 574.Pt 1, pp. 283–290.

Katz, L. C. and Shatz, C. J. (1996). "Synaptic activity and the construction of cortical circuits." *Science* 274.5290, pp. 1133–1138.

Kip, Sertac N et al. (2006). "Changes in the expression of plasma membrane calcium extrusion systems during the maturation of hippocampal neurons." *Hippocampus* 16.1, pp. 20–34.

Konur, Sila and Ghosh, Anirvan (2005). "Calcium signaling and the control of dendritic development." *Neuron* 46.3, pp. 401–405.

Kwon, Hyung-Bae and Sabatini, Bernardo L. (2011). "Glutamate induces de novo growth of functional spines in developing cortex." *Nature* 474.7349, pp. 100–104.

Lai, Cora Sau Wan, Franke, Thomas F., and Gan, Wen-Biao (2012). "Opposite effects of fear conditioning and extinction on dendritic spine remodelling." *Nature* 483.7387, pp. 87–91.

Langston, Rosamund F. et al. (2010). "Development of the spatial representation system in the rat." *Science* 328.5985, pp. 1576–1580.

Lavenex, P. and Amaral, D. G. (2000). "Hippocampal-neocortical interaction: a hierarchy of associativity." *Hippocampus* 10.4, pp. 420–430.

Lee, S. H. et al. (2000). "Differences in Ca^{2+} buffering properties between excitatory and inhibitory hippocampal neurons from the rat." *J Physiol* 525 Pt 2, pp. 405–418.

Liao, C. W. and Lien, C. C. (2009). "Estimating intracellular Ca^{2+} concentrations and buffering in a dendritic inhibitory hippocampal interneuron." *Neuroscience* 164.4, pp. 1701–1711.

Liotta, Agustin et al. (2012). "Energy demand of synaptic transmission at the hippocampal Schaffer-collateral synapse." *J Cereb Blood Flow Metab* 32.11, pp. 2076–2083.

Lohmann, Christian, Finski, Alexei, and Bonhoeffer, Tobias (2005). "Local calcium transients regulate the spontaneous motility of dendritic filopodia." *Nat Neurosci* 8.3, pp. 305–312.

Losonczy, Attila, Makara, Judit K., and Magee, Jeffrey C. (2008). "Compartmentalized dendritic plasticity and input feature storage in neurons." *Nature* 452.7186, pp. 436–441.

Lytton, Jonathan et al. (2002). "K^+-dependent Na^+/Ca^{2+} exchangers in the brain." *Ann N Y Acad Sci* 976, pp. 382–393.

Magee, J. C. and Johnston, D. (1997). "A synaptically controlled, associative signal for Hebbian plasticity in hippocampal neurons." *Science* 275.5297, pp. 209–213.

Mainen, Z. F., Malinow, R., and Svoboda, K. (1999). "Synaptic calcium transients in single spines indicate that NMDA receptors are not saturated." *Nature* 399.6732, pp. 151–155.

Majewska, A., Tashiro, A., and Yuste, R. (2000). "Regulation of spine calcium dynamics by rapid spine motility." *J Neurosci* 20.22, pp. 8262–8268.

Maravall, M. et al. (2000). "Estimating intracellular calcium concentrations and buffering without wavelength ratioing." *Biophys J* 78.5, pp. 2655–2667.

McBain, C. J., Freund, T. F., and Mody, I. (1999). "Glutamatergic synapses onto hippocampal interneurons: precision timing without lasting plasticity." *Trends Neurosci* 22.5, pp. 228–235.

Miller, M. (1981). "Maturation of rat visual cortex. I. A quantitative study of Golgi-impregnated pyramidal neurons." *J Neurocytol* 10.5, pp. 859–878.

Neher, E. and Augustine, G. J. (1992). "Calcium gradients and buffers in bovine chromaffin cells." *J Physiol* 450, pp. 273–301.

Normann, C. et al. (2000). "Associative long-term depression in the hippocampus is dependent on postsynaptic N-type Ca^{2+} channels." *J Neurosci* 20.22, pp. 8290–8297.

Papa, Michele et al. (2003). "Differential expression of the Na^+-Ca^{2+} exchanger transcripts and proteins in rat brain regions." *J Comp Neurol* 461.1, pp. 31–48.

Patterson, Michael, Sneyd, James, and Friel, David D. (2007). "Depolarization-induced calcium responses in sympathetic neurons: relative contributions from Ca^{2+} entry, extrusion, ER/mitochondrial Ca^{2+} uptake and release, and Ca^{2+} buffering." *J Gen Physiol* 129.1, pp. 29–56.

Pohle, Jörg (2007). *Quantitatives Calcium-Imaging an hippocampalen Gliazellen.* Diploma thesis.

Purves, Dale et al. (2008). *Principles of cognitive neuroscience.* Sinauer.

Raymond, Clarke R. (2007). "LTP forms 1, 2 and 3: different mechanisms for the "long" in long-term potentiation." *Trends Neurosci* 30.4, pp. 167–175.

Regehr, W. G. and Tank, D. W. (1994). "Dendritic calcium dynamics." *Curr Opin Neurobiol* 4.3, pp. 373–382.

Romand, Sandrine et al. (2011). "Morphological development of thick-tufted layer v pyramidal cells in the rat somatosensory cortex." *Front Neuroanat* 5, p. 5.

Rozsa, Balazs et al. (2004). "Distance-dependent scaling of calcium transients evoked by backpropagating spikes and synaptic activity in dendrites of hippocampal interneurons." *J Neurosci* 24.3, pp. 661–670.

Sabatini, B. L. and Svoboda, K. (2000). "Analysis of calcium channels in single spines using optical fluctuation analysis." *Nature* 408.6812, pp. 589–593.

Sabatini, Bernardo L., Oertner, Thomas G., and Svoboda, Karel (2002). "The life cycle of Ca^{2+} ions in dendritic spines." *Neuron* 33.3, pp. 439–452.

Sandler, V. M. and Barbara, J. G. (1999). "Calcium-induced calcium release contributes to action potential-evoked calcium transients in hippocampal CA1 pyramidal neurons." *J Neurosci* 19.11, pp. 4325–4336.

Scheuss, Volker et al. (2006). "Nonlinear $[Ca^{2+}]$ signaling in dendrites and spines caused by activity-dependent depression of Ca^{2+} extrusion." *J Neurosci* 26.31, pp. 8183–8194.

Schmidt-Hieber, Christoph, Jonas, Peter, and Bischofberger, Josef (2004). "Enhanced synaptic plasticity in newly generated granule cells of the adult hippocampus." *Nature* 429.6988, pp. 184–187.

Seifert, Gerald et al. (2009). "Analysis of astroglial K^+ channel expression in the developing hippocampus reveals a predominant role of the Kir4.1 subunit." *J Neurosci* 29.23, pp. 7474–7488.

Sipilä, Sampsa T. et al. (2009). "Compensatory enhancement of intrinsic spiking upon NKCC1 disruption in neonatal hippocampus." *J Neurosci* 29.21, pp. 6982–6988.

Spitzer, Nicholas C (2006). "Electrical activity in early neuronal development." *Nature* 444.7120, pp. 707–712.

Spruston, N. et al. (1995). "Activity-dependent action potential invasion and calcium influx into hippocampal CA1 dendrites." *Science* 268.5208, pp. 297–300.

Stocca, Gabriella, Schmidt-Hieber, Christoph, and Bischofberger, Josef (2008). "Differential dendritic Ca^{2+} signalling in young and mature hippocampal granule cells." *J Physiol* 586.16, pp. 3795–3811.

Stuart, G. and Häusser, M. (1994). "Initiation and spread of sodium action potentials in cerebellar Purkinje cells." *Neuron* 13.3, pp. 703–712.

Stuart, G., Schiller, J., and Sakmann, B. (1997). "Action potential initiation and propagation in rat neocortical pyramidal neurons." *J Physiol* 505, pp. 617–632.

Stuart, G. et al. (1997). "Action potential initiation and backpropagation in neurons of the mammalian CNS." *Trends Neurosci* 20.3, pp. 125–131.

Stuart, G. J. and Sakmann, B. (1994). "Active propagation of somatic action potentials into neocortical pyramidal cell dendrites." *Nature* 367.6458, pp. 69–72.

Tank, D. W., Regehr, W. G., and Delaney, K. R. (1995). "A quantitative analysis of presynaptic calcium dynamics that contribute to short-term enhancement." *J Neurosci* 15.12, pp. 7940–7952.

Thayer, Stanley A., Usachev, Yuriy M., and Pottorf, William J. (2002). "Modulating Ca^{2+} clearance from neurons." *Front Biosci* 7, pp. 1255–1279.

Vogel-Ciernia, Annie et al. (2013). "The neuron-specific chromatin regulatory subunit BAF53b is necessary for synaptic plasticity and memory." *Nat Neurosci.*

Wallraff, Anke et al. (2006). "The impact of astrocytic gap junctional coupling on potassium buffering in the hippocampus." *J Neurosci* 26.20, pp. 5438–5447.

Wasling, Pontus, Hanse, Eric, and Gustafsson, Bengt (2002). "Long-term depression in the developing hippocampus: low induction threshold and synapse non-specificity." *J Neurosci* 22.5, pp. 1823–1830.

Waters, Jack and Helmchen, Fritjof (2004). "Boosting of action potential backpropagation by neocortical network activity in vivo." *J Neurosci* 24.49, pp. 11127–11136.

Waters, Jack, Schaefer, Andreas, and Sakmann, Bert (2005). "Backpropagating action potentials in neurones: measurement, mechanisms and potential functions." *Prog Biophys Mol Biol* 87.1, pp. 145–170.

Wilbrecht, Linda et al. (2010). "Structural plasticity underlies experience-dependent functional plasticity of cortical circuits." *J Neurosci* 30.14, pp. 4927–4932.

Wills, Tom J. et al. (2010). "Development of the hippocampal cognitive map in preweanling rats." *Science* 328.5985, pp. 1573–1576.

Wittenberg, Gayle M and Wang, Samuel S-H (2006). "Malleability of spike-timing-dependent plasticity at the CA3-CA1 synapse." *J Neurosci* 26.24, pp. 6610–6617.

Wong, Rachel O L. and Ghosh, Anirvan (2002). "Activity-dependent regulation of dendritic growth and patterning." *Nat Rev Neurosci* 3.10, pp. 803–812.

Woodhall, G. et al. (1999). "Membrane potential and intracellular Ca^{2+} oscillations activated by mGluRs in hippocampal stratum oriens/alveus interneurons." *J Neurophysiol* 81.1, pp. 371–382.

Xia, Zhengui and Storm, Daniel R. (2005). "The role of calmodulin as a signal integrator for synaptic plasticity." *Nat Rev Neurosci* 6.4, pp. 267–276.

List of Figures

2.1 Medial temporal lobe 8
2.2 Morphology of hippocampus 9
2.3 Place cells and theta rhythm 10
2.4 The hippocampal formation 11
2.5 Interaction of PFC and CA1 12
2.6 Developmental changes in the morphology of dendrites . . . 13
2.7 Ca^{2+} as signal molecule for dendritic development 15
2.8 Dendritic backpropagation of action potentials 17
2.9 Expression of PMCAs during development 18

3.1 The one-compartment model 24
3.2 Free vs bound Ca^{2+}, buffer saturation 26
3.3 Consequences of the one-compartment model 29

4.1 Biocytin filled pyramidal cells 32
4.2 Amplitudes in control vs. TTX in young neurons 33
4.3 Amplitudes in control vs. TTX in mature neurons 34
4.4 Action potentials vs mock action potentials in TTX 35
4.5 Rapid postnatal development of Ca^{2+} 36
4.6 Ca^{2+} transients with different Fura concentrations 37
4.7 Buffer capacity experiments 39
4.8 Decay rates scales linearly with amplitude of Ca^{2+} transients during brief bursts of AP 40
4.9 Decay time constants are independent of AP numbers in brief bursts 41
4.10 Linear summation of dendritic Ca^{2+} transients during brief bursts of APs 42
4.11 Activity dependent slow-down of extrusion during theta burst firing 43
4.12 Decay phase after Ca^{2+} transient induced by TBS_{10} 45
4.13 Effective temporal summation of dendritic Ca^{2+} transients in young cells 46
4.14 Ca^{2+} per spike 47

5.1 Activity-dependent slowing of the decay of $[Ca^{2+}]_i$ 51

List of Tables

4.1 Results of buffer capacity experiment 39

5.1 Comparison of buffer capacities with literature 49

Nomenclature

$[Ca^{2+}]_{rest}$	resting Ca^{2+} concentration, usually 40-60 nM in pyramidal neurons, 26
$\Delta[Ca^{2+}]_i$	elevation of free Ca^{2+} above resting Ca^{2+} concentration, 26
$\Delta[Ca^{2+}]_T$	total calcium load, change in total Ca^{2+} concentration, i.e free and bound Ca^{2+}, 25
γ	Ca^{2+} extrusion rate (Ca^{2+} clearance rate), removal of free intracellular Ca^{2+} from the cytosol, 27
κ_B	Ca^{2+} buffer capacity (Ca^{2+} binding ratio) of exogenous buffer, here: Fura, 26
κ_S	Ca^{2+} buffer capacity (Ca^{2+} binding ratio) of endogenous buffer, 26
τ	decay time constant of Ca^{2+} transient, i.e. after the duration of τ the amplitude decays to $\frac{1}{e}$ of the maximal amplitude, 28
τ_0	decay time constant of Ca^{2+} transient with no exogenous Ca^{2+} buffer prolonging the decay, 29
τ_1	average decay time constant of brief Ca^{2+} transients measured with 100-200 µM Fura-FF, 30
A_0	Ca^{2+} amplitude with no exogenous Ca^{2+} buffer reducing the amplitude, 29
A_1	average Ca^{2+} amplitude measured with 100-200 µM Fura-FF, 30
K_d	dissociation constant, 23
r	linear correlation coefficient, 41
AMPA receptors	2-amino-3-(3-hydroxy-5-methyl-isoxazol-4-yl)propanoic acid receptors, ionotropic glutamate receptors, generation of excitatory postsynaptic potentials, 58

APs	action potentials, in our measurements evoked via current injections using patch clamp whole-cell mode of a neuron in current clamp, 6
bAP	backpropagating action potential, 16
CA1	Cornu Ammonis area 1, subregion of the hippocampus, 7
CA3	Cornu Ammonis area 3, subregion of the hippocampus, 7
EPSP	excitatory postsynaptic potential, 17
Fura-2	high-affinity ratiometric Ca^{2+} indicator (dye), K_d=0.286 nM, 17
Fura-FF	low-affinity ratiometric Ca^{2+} indicator (dye), K_d=4.18 µM, 20
LTD	long-term depression, 58
LTP	long-term potentiation, 58
Na_v	voltage-gated sodium channels, 6
NCX, NCKX	Na^+-Ca^{2+} exchangers, Na^+-K^+-Ca^{2+} exchangers, 56
NMDA receptors	N-Methyl-D-aspartic acid/N-Methyl-D-aspartate receptors, ionotropic glutamate receptors which are important for synaptic plasticity, 15
Pn	postnatal day n, 11
PMCAs	plasma-membrane ATPases, i.e. pumps which transport Ca^{2+} from the cytosol into extracellular space, 18
Ras	small GTPases that are involved in cellular signal transmission, 57
SEM	standard error of the mean, 33
SERCA	smooth endoplasmatic reticulum Ca^{2+} ATPases, pump Ca^{2+} from the cytosol into smooth endoplasmatic reticulum, 18
TBS_n	theta-burst stimulation, here: a 100 Hz burst of n evoked action potentials, repeated 10-times at 5 Hz (∼theta frequency), 30
TTX	Tetrodotoxin, blocks voltage-gated, fast sodium channels, 17